Fabrication of a light-weight SOFC using ceramic fibre paper as substrate

CENTRE FOR ANALYSIS AND SYNTHESIS | FACULTY OF ENGINEERING | LUND UNIVERSITY
PHILIP LÖFKVIST | MASTER OF SCIENCE THESIS | 2015

Fabrication of a light-weight SOFC using ceramic fibre paper as substrate

Master of Science Thesis

Centre for analysis and synthesis
Faculty of Engineering
Lund University

LUND UNIVERSITY

Philip Löfkvist

2015-10-16

Supervisors:
Dr. Fredrik Silversand, Catator
Prof. Reine Wallenberg, Lund University

Examiner:
Prof. Jan-Olle Malm, Lund University

Abstract

A novel method for the fabrication of a light-weight solid oxide fuel cell (SOFC) has been evaluated at Catator. This was conducted in order to lower the weight and thus cost of an unmanned aerial vehicle (UAV). The main aim for this thesis was to achieve a thin, dense and crack-free electrolyte using a ceramic fibre paper as substrate. This paper was impregnated with colloidal solutions and pressed to planar and tubular structures to achieve a porous substrate for the SOFC. Nickel was incorporated and a bilayer was coated on top of the substrate to create a flat surface onto which a thin electrolyte and cathode layer could be applied. All steps were followed by heat treatments to enable drying, calcination or sintering processes. Scanning electron microscopy (SEM) and energy dispersive spectroscopy (EDS) were used to investigate the characteristics of the electrolyte and the chemical make-up of the SOFC respectively. Optical microscopy (OM) was used extensively to get an understanding of how the different experimental methods were affecting the microstructure. A system test was performed by constructing a test oven but failed due to malfunctions which was probably caused by short circuits. The results from the SEM indicates that the electrolyte was quite dense but not free from cracks and the EDS shows an unevenly distributed anode. If the desired outcome is to be achieved using similar methods an automated process need to be implemented since it is currently too time consuming to be cost effective. A weight decrease of 50 % was observed compared to a conventional SOFC previously used by Catator, so if a working method could be achieved there could be decreases in cost for mobile applications.

Sammanfattning

En ny metod för tillverkningen av en lågvikts-fastfasbränslecell (SOFC) har genomförts hos Catator AB. Detta gjordes för att kunna minska vikten och därmed kostnaden hos en obemannad luftfarkost. Det främsta målet för den här uppsatsen var att åstadkomma ett tunt, kompakt och sprickfritt elektrolytlager genom användandet av ett keramiskt fiberpapper som grundstruktur. Detta papper impregnerades med kolloidala lösningar följt av pressning till plana och rörformiga strukturer för att åstadkomma ett poröst substrat. Nickel innefattades i substratet varpå ett dubbellager applicerades ovanpå detta för att skapa en jämn yta på vilken ett tunt elektrolyt- och katodlager senare kunde appliceras. Alla olika steg följdes av värmebehandlingar för att åstadkomma torkning, kalcinering eller sintring. Svepelektronmikroskopi (SEM) användes för att undersöka elektrolytens utseende och röntgenspektroskopi (EDS) för att se den kemiska sammansättningen i bränslecellen. Ljusmikroskopi användes flitigt för att få en förståelse för hur de olika experimentella delarna påverkar mikrostrukturen. För att se om de tillverkade bränslecellerna fungerade gjordes en testugn. Dock misslyckades dessa försök, antagligen på grund av kortslutningar i systemet. Resultaten från SEM och EDS visade ett hyfsat tätt elektrolytmembran och en ojämn nickelfördelning i anoden. För att uppnå det önskade målet genom användandet av liknande metoder måste en automatiserad process implementeras då de för tillfället är för tidskrävande för att vara kostnadseffektiva. En viktminskning av 50 % har uppnåtts jämfört med konventionella SOFC som tidigare använts av Catator AB, så om en fungerande metod kan användas skulle det betyda en kostnadsminskning för mobila applikationer.

Acknowledgement

I would hereby like to express my sincerest gratitude to the people involved in the making of this thesis. Below are some of the people that helped me during the course of my project:

Fredrik, for giving me guidance and supervision during my time at Catator.

Reine, for giving me advises, supervision and assistance during the SEM sessions.

Tian, for assisting me during chemical and material orderings.

Mariano, for giving me tips about writing the thesis but mostly for lifting the working spirit by randomly speaking Italian on the phone.

Yasir, for giving me advice in the lab.

Mikael, for always being there when I needed help with technical difficulties.

Jörgen, for providing me with technical tips along the experimental part of the thesis and creating the test oven used for the performance tests.

Putte, for assisting me in the workshop.

Paula, for assisting me with printing.

I would also like to thank my family and friends for their continuing support and understanding.

Table of Contents

1 Introduction

A fuel cell is a device capable of converting the chemical energy of a fuel directly into electrical energy [1]. Since this process doesn't involve any moving parts, i.e. transformation into mechanical energy, higher efficiencies can be achieved compared to e.g. combustion engines [2]. SOFCs have the highest efficiency of all fuel cells and are thus more environmentally friendly. They also have greater fuel flexibility [3].

The first fuel cell was invented in 1838 by William Grove. The research efforts has been growing ever since and exponentially in the last 20 years. Given the vast history of fuel cells it has not yet reached the desired outcome of being an integrated highly efficient power generator in our society. The main difficulty for this is the expensive manufacturing related to materials and processing. It is simply not cost-effective yet. However fuel cells are anticipated to have great implications in the near future when the key problems have been solved [4] [5].

A fuel cell basically consists of many connected units to form what is called a stack. Each unit comprises an anode, electrolyte and cathode. SOFCs can be divided in to two groups based on their physical form, namely planar and tubular. Planar SOFCs are easier to manufacture, have a higher power density and are most suited for stationary applications such as power generators. Tubular SOFCs on the other hand are generally cheaper to produce, easier to seal and are most suited for mobile applications such as RVs and unmanned aerial vehicles due to their fast start-up and shut down capabilities [6] [7]. If the weight of a UAV and other small scale power generators could be lowered it would be more energy efficient. It would therefore be of interest to manufacture SOFCs that have a lower weight with the same power output.

This thesis aims to manufacture a light weight SOFC unit at Catator which could be used in a UAV. The SOFC will be using a ceramic fibre paper as framework, a nickel and yttria stabilized zirconia (YSZ) based anode and a YSZ electrolyte. The cathode application will be based on earlier work done by Catator [8]. The anode will be applied with a sol-gel technique. A method for applying a dense and crack-free electrolyte will be assessed and SEM as well as EDS will be used to evaluate the method. Performance tests will also be conducted to evaluate the function of the SOFC. The main work will be done at Catator and the advanced characterization at Lund University.

2 Theory

2.1 Fuel cells

A fuel cell with an electrolyte that transports oxygen ions and uses hydrogen as fuel can be described in the following way: The hydrogen is catalytically dissociated and oxidized at the anode at which electrons are produced and guided via external circuits to the cathode. At the cathode, oxygen gas from air is catalytically dissociated and reduced into oxygen ions using the electrons from the anode, see Formula 1. These oxygen ions are transported through the electrolyte to the anode, where they together with the anode material oxidize hydrogen and form electrons and water which completes the circle, see Formula 2. The created current of electrons passing from the anode to the cathode via interconnects are used to power the current system used. See Figure 1 for an elementary understanding.

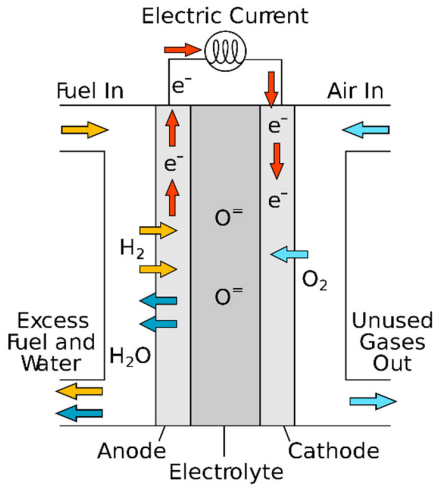

Figure 1. The principal workings of a dscj cell [9].

$$O_2 + 4e^- \rightarrow 2O^{2-} \quad (1)$$

$$H_2 + O^{2-} \rightarrow H_2O + 2e^- \quad (2)$$

The basis of a fuel cell's operation is utilized through the mechanism of ion conductivity of the electrolyte. The varying types of fuel cells are categorized by the media in which this process take place. The most common fuel cells are: SOFC, polymer electrolyte membrane fuel cell (PEMFC), direct methanol fuel cell (DMFC), alkaline fuel cell (AFC), phosphoric acid fuel cell (PAFC) and molten carbonate fuel cell (MCFC). These can be compared in Table 1 below, note that these are their most common characteristics and exceptions exists.

Table 1. Comparison between different fuel cells and their most common attributes [10] [11].

	PEMFC	AFC	PAFC	MCFC	SOFC
Electrolyte	Polymer (Fluorinated sulfonic acid polymer)	35-85% concentrated KOH in a matrix of asbestos	100% concentrated phosphoric acid	Molten alkali carbonates in a solid $LiAlO_2$ matrix	Solid and dense ceramic
Operating temperature	40-80 °C	50-220 °C	150-220 °C	600-700 °C	400-1000 °C
Catalyst	Pt	-Pt -Ni -Ag	Pt	Ni / NiO	Ni / Perovskite
Ion carried through electrolyte	H^+	OH^-	H^+	CO_3^{2-}	O^{2-}
Maximum Efficiency	60%	60%	55%	65%	65%
Start-up time	Minutes	Minutes	Minutes	Hours	Hours
Advantages	-High power density -Minimal corrosion problems	Wide range of catalysts	Less CO sensitive than PEMFC and AFC	No expensive catalysts	-High efficiency -Fuel flexible, including CO
Problems	-Water balance -Sensitive to CO and S	If air is used CO_2 must be removed -CO sensitive	-Corrosive electrolyte -CO sensitive	-Corrosive and mobile electrolyte	Corrosion

2.1.1 Solid Oxide Fuel Cells

SOFCs operates at high temperatures (400-1000 °C) [5]. This high temperature is required for the sufficient conduction of ions through the membrane which increases with temperature. It is the high temperature that allows the SOFC to be superior in efficiency compared to other fuel cells since the reaction mechanisms are faster and the waste heat can be used more efficiently. At this temperature there is also a sufficient reaction rate with non-noble metal catalysts, thus lowering the cost of the anode and cathode [12]. This however put a higher strain on the internal materials used since they have to withstand the occurring oxidizing and reducing environments during these high temperatures [5]. Generally SOFC have a required operation time of 40 000 h. For this project however the duration is not as important and set around 100 h.

SOFCs can either be electrolyte supported or electrode supported (i.e. anode or cathode supported), see images below. The total cell thickness varies between 0.2-2mm, with the electrolyte supported generally being towards the thinner spectrum [4]. Due to non-mechanically stable electrodes

produced before the 21st century the planar fuel cells were primarily electrolyte supported. These electrolytes typically had a thickness of 100-200µm which required temperatures above 1000°C in order to conduct enough oxygen ions through the membrane [13]. Nowadays however an anode supported approach is the most common which can allow a thinner electrolyte layer (10-20µm) which in turn can lower the operation temperature to 400-700 °C.

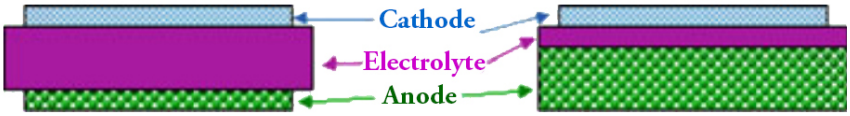

Figure 2. The basic difference between an electrolyte supported and an anode supported SOFC [6].

The most common SOFC consists of a porous anode-supported Ni-YSZ, a thin dense YSZ electrolyte membrane and a porous lanthanum strontium manganite (LSM) cathode. Although this is the most common material choice for SOFCs a brief list of alternatives will be given in the following pages.

The reactions for a SOFC occurs at the so called triple phase boundaries (TPB) where ions, electrons and gas (either hydrogen or oxygen) coexist. This takes place where there is gas and a connection between the electron conducting material and the ionic conducting material, see Figure 3 below. For achieving a high degree of TPB it thus becomes important that the reactive parts consists of small grains of the different materials in order to increase the solid boundaries as well as having a porous structure to increase the gas phase boundary [14].

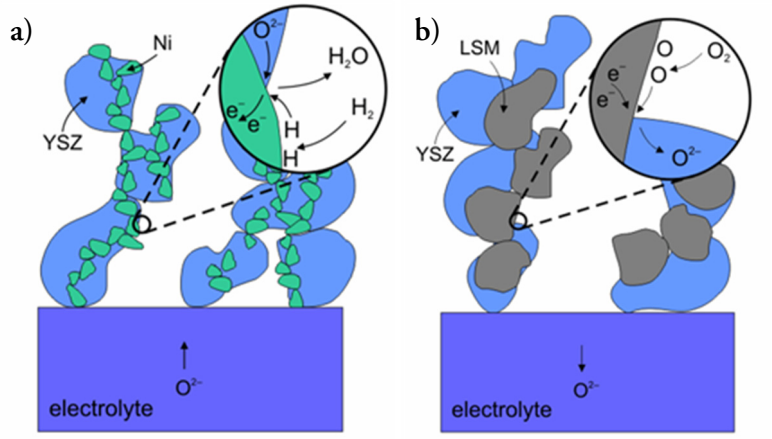

Figure 3. Illustration of the TPB for a) the anode and b) the cathode [15].

2.1.1.1 Anode

As mentioned above the anode need to be porous in order to increase the TPB but also to facilitate gas transport from outside of the cell to the reactive sites through the anode structure. Other important criteria for the anode is the following: Being an effective catalyst for fuel oxidation, high electron conductivity, having a matching TEC with the electrolyte as well as being stable in reducing and oxidizing environments, which occurs during operation and manufacturing

respectively [1]. In the table below some anode materials which follow these critical properties are presented.

Table 2. A comparison between different anode materials used in SOFCs [1] [5] [16] [17] [18].

Anode Material	**Advantages**	**Limitations**
Platinum-Gold (Pt-Au)	-High catalytic activity -High electronic conductivity	-Very expensive
Nickel-YSZ (Ni-YSZ)	-Excellent catalytic activity for oxidizing the fuel -Conducts electrons well	-Volume changes during redox cycles -Low tolerance to sulphur
Copper-Ceria (Cu-CeO_2)	-Can reform hydrocarbons, more fuel flexible -Has better sulphur resistance than Ni	-Copper coarsening at operating temperatures -Difficult to integrate with existing manufacturing processes
LSCM ($La_{0.75}Sr_{0.25}Cr_{0.5}Mn_{0.5}O_3$)	-Redox stability -Good conductivity and reaction kinetics	-Low catalytic activity compared to Ni

The most common anode material is made of Ni and YSZ. This mixture is usually made by fine particulate powders pressed together to form what is called a cermet. A cermet consists of a microscopic blend of a metal and a ceramic material which gives it mixed metallic and ceramic properties [14]. The reason for blending in YSZ in the nickel anode is to get a more similar TEC to the electrolyte and to reduce the sinterability and coarsening of nickel grains which can occur at elevated temperatures [13]. The most common fabrication methods for the anode is through pellet-pressing powders under high pressure or cylindrically extruding a thick paste for planar and tubular SOFC respectively.

Ceria has been investigated as an addition to the Ni-YSZ cermet. It has been shown that impregnation of ceria in to the anode can cause oxidative catalysis, oxygen ion conductivity as well as some electronic conductivity in reducing environments [14] [19]. It's a bit contradictive however since some researchers says that it decreases the overall efficiency of the SOFC while some have said it increases it [20] [21]. Nevertheless some samples in this project were impregnated with ceria due to its positive properties.

2.1.1.2 Electrolyte

The electrolyte, also denoted here as membrane, is perhaps the most crucial part of the whole SOFC. There are certain criteria that needs to be fulfilled for an electrolyte working at high temperatures (600-1000 °C). The primary ones are listed below, it should have:

- High ionic and negligible electronic conduction in order to transport the oxygen ions while hindering the flow of electrons [22].

- A TEC that is in proximity with that of the anode and cathode to avoid tension which can lead to cracking [5].
- Chemical stability at oxidizing and reducing environments at high temperatures, which occurs at the cathode and anode respectively [23].
- Negligible inter-diffusion and reactions with the anode or cathode [4].
- Dense structure, i.e. free of cracks and pores to ensure that no gas leaks through the membrane [5].

In order to achieve a dense, pore free electrolyte membrane, high temperature sintering is required, which fuses the grains together. This process shrinks the electrolyte which can produce tension which in turn can cause the membrane to crack. Keeping a low heating rate will aid in this matter. Some electrolyte materials used in SOFCs are shown in the table below.

Table 3. Typical electrolyte materials are compared [4] [16] [23] [24] [25] [26].

Name	**Operating temperature**	**Pros**	**Cons**
YSZ $(Y_2O_3)_{0.08}(ZrO_2)_{0.92}$	800-1000 °C	-Great mechanical properties -Stability in oxidized and reduced environments	-Relatively bad oxygen conduction -High temperatures are needed
Scandia stabilized zirconia $(Sc_2O_3)_{0.2}(ZrO_2)_{0.8}$	500-600 °C	Very good oxygen conductivity and mechanical strength	Problems with phase transition at 600-700 °C, aging as well as cost
Gadolinia, samaria and yttria doped ceria $Ce_{0.8}Gd_{0.2}O_{1.8}$ $Ce_{0.8}Sm_{0.2}O_{1.9}$ $Ce_{0.8}Y_{0.2}O_{1.96}$	500-700 °C	Very good oxygen conductivity	-Relatively low mechanical strength -Unstable at low oxygen partial pressures -Densification req. temp. >1500 °C -Short circuit T>700 °C due to electrical conductivity
LSGMC	600-800 °C	Very good oxygen conduction	-Ga evaporation at reducing environments -Thin film formation is difficult
YSB	400-800 °C	Very good oxygen conduction	-Not researched enough -Expensive

In order for a material to conduct oxygen ions it needs to contain certain defects [27]. The inherent structure of the membrane is usually fluorite or perovskite altered in such ways that either vacancy or interstitial defects are present. This makes it possible for oxygen anions to travel from vacancy

to vacancy throughout the lattice from the cathode to the anode. The oxygen anion conductivity has been shown to be affected by the crystal lattice size [12].

Since stabilized zirconia is the most common lattice material used a brief description of the stabilization will be presented. Zirconia can exist in three different morphologies. At 1170°C the structure changes from monoclinic to tetragonal and further to a fluorite structure above 2370°C. These reversible changes happens very rapidly without diffusion and can cause volume changes during cooling which can generate cracks [4] [28]. The addition of oxides with a different valence, especially the rear-earth metals, can stabilize the zirconia in the fluorite structure [27]. In order to achieve a high conductivity of oxygen ions in zirconia-based electrolytes the addition of cationic dopants needs to be sufficient in order to stabilize the fluorite structure and to create interstitial defects. However, adding to much dopant and the ionic conductivity decreases due to coalescence of oxygen vacancies and dopant cluster formation [22]. 8 mol% Y_2O_3 in ZrO_2 is the most common compositional concentration used [6].

2.1.1.3 Cathode

As mentioned before, the cathode is responsible for the reduction of oxygen and transporting them to the electrolyte. In order to fulfil this and to work properly there are some criteria that needs to be met. They are as follows: High conduction of electrons, the ability to catalytically dissociate and reduce oxygen molecules, similar TEC as the anode and electrolyte, minimum reaction with the electrolyte as well as being stable in an oxidizing environment at elevated temperatures. The microstructure need to be porous for the same reason as the anode, to facilitate the diffusion of oxygen through the matrix and increasing the TPB [29]. The most commonly used cathode for SOFC is LSM. The cathode used in this project will be based on the previous work at Catator done by Marcus Andersson which used LSM-YSZ and LSM [8].

2.2 Project description

2.2.1 Anode formation

Since this project will be using a ceramic fibre paper as substrate the conventional methods of fabrication, i.e. powder pressing and extrusion, cannot be applied. Another way to create a mechanically stable substrate is therefore needed. One way of achieving this is by impregnating the fibre paper with a colloidal solution. Upon drying the solution will form a sol-gel which after calcination will form a layer around the fibres thus creating a more stable structure.

Nickel needs to be incorporated in to the substrate as an oxide powder or salt solution. When pressing oxide powders together the lowest amount of nickel needed in order to create a continuous network and provide electron conductivity throughout the entire matrix is around 30 vol%. This is based on randomly arranging powders together tightly. When looking at more porous matrixes, like the one used in this project the same principle does not apply. Since the nickel is not randomly distributed through the anode but preferably situated at the fibre walls of the substrate the critical

factor becomes how evenly distributed the nickel is as well as its thickness along the walls. This becomes clearer if we look at the microstructure, see figure 4 on the next page.

The incorporated nickel will become NiO during calcination. In order for the anode to become electronically conductive the NiO need to be reduced to metallic Ni. This will cause a reduction in the volume which will produce a more porous microstructure. This is accomplished by heating up to 600-800 °C in a reducing environment which is usually a mixture of hydrogen and nitrogen [30] [31].

A word on caution. Nickel has the following health classifications: May cause cancer upon inhalation (R49) and may cause sensitization upon skin contact (R43). Appropriate safety gears should thus be implemented during experiments. Nickel can at low temperatures react with CO to form a very toxic carbonyl compound which is lethal even in low concentrations. This compound will not be formed during this project but is considered to be one of the most dangerous industrial chemicals [32].

2.2.2 Ceramic fibre paper

Ceramic fibre papers are quite commonly used as ceramic structures in catalysis applications [33]. It is also used as insulation for numerous technical devices due to its open structure and high heat resistance. The concept of a ceramic paper as a structured backbone for a fuel cell, as used in this project, has however not been reported in the literature. The closest finds I have made are the two following: Nickel impregnated homemade ceramic paper has been used as a catalyst for a SOFC and zirconia fibres have been used as an anode structure [21] [34]. An electrolyte supported SOFC was used in these cases as opposed to the anode supported approach used in this project.

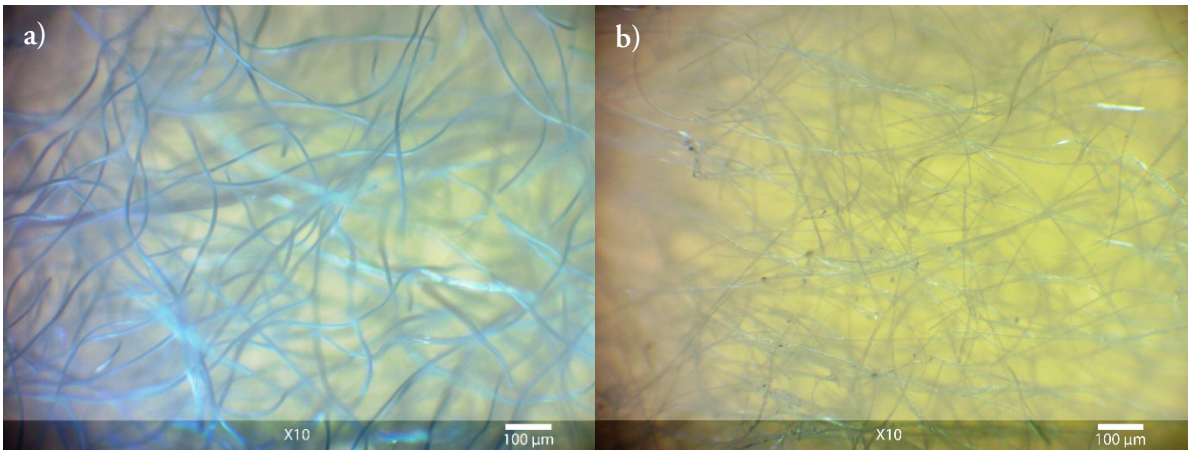

Figure 4. a) YSZ and b) alumina ceramic fibre paper magnified 10 times revealing their fibrous network.

The microstructure is similar to that of regular paper and consists of connected ceramic fibres which form a low density 3d-network, see Figure 4 above. This offers a flexibility of the shape, especially if a binder is incorporated [35]. The ceramic paper commonly consists of alumina deposited on top of a mixture of alumina and silica fibres, but the chemical composition can vary [35] [36]. For this

project however an alumina and a 10-YSZ ceramic paper will be used. Their constituents are listed in the table below. The 10-YSZ contains 10 mol% yttria.

Table 4. Specific make-up of the ceramic fibre papers used in this project as supplied by Zircar Zirconia, Inc. [37].

Ceramic fibre paper	YSZ / wt%	Alumina / wt%	Silica / wt%	Binder / wt%	Fibre thickness / μm
10-YSZ	99+	<0.01	<0.02	0	4-6
Alumina	0	80	5	15	6

The reason for using two different ceramic papers are due to their different properties. The 10-YSZ have a similar TEC as the electrolyte and the alumina is more light-weighted and easier to handle.

2.2.3 Anode Functional Layer

The anode functional layer (AFL) is a layer between the anode and the electrolyte. It is not very common but nonetheless used in some applications. It can be used to increase the TPB, prevent reactions between the anode and the electrolyte, increase the catalytic performance of the anode and reduce the electrode polarization resistance. It can also be used to separate the electronically conducting phase from the catalytically active one and thereby reducing the amount of catalyst needed [14] [28] [31] [38].

The AFL can be deposited using techniques such as wet powder spraying, vacuum slip casting, screen printing, dip coating and paint brushing [3] [38] [39].

Since the substrate in this project is a porous fibrous network and the method of choice for the electrolyte application is dip-coating there need to be something on top of the substrate. This is where the AFL comes in; it provides the necessary building ground for the electrolyte. Without it the electrolyte solution would just absorb into the matrix of the substrate and not create a continuous film.

In this project the AFL was applied as a paste which either had been ball-milled and/or ultra-sonicated. Ball-milling is used to minimize particle size and agglomeration as well as providing homogeneous mixing. It utilizes the grinding effect of ceramic balls in a rotating cylindrical container. Ultra-sonication uses sound waves to minimize particle agglomeration as well as providing some mixing. Entrapped air bubbles can also be removed by this technique.

2.2.4 Electrolyte application

The most crucial part in the fabrication of a fuel cell is the manufacture of a dense electrolyte membrane [40]. The critical properties of the membrane are strongly related to its microstructure [6]. In order to achieve the desired microstructure an adequate synthesize method is required. There

are numerous ways of creating a thin, dense electrolyte layer on top of a porous structure. In the table below some common techniques as well as their strengths and drawbacks are depicted.

Table 5. Different methods for electrolyte applications including their pros and cons [41] [42] [43].

Application technique	**Advantages**	**Disadvantages**
Electrochemical vapour deposition	Reliable to achieve thin dense electrolyte layer	-Low deposition rates -Pricey equipment
Chemical vapour deposition		
Physical vapour deposition		
Thermal spraying	High deposition rates	Unreliable in achieving a dense electrolyte layer
Sol-gel	Thin layers can be achieved	-Repeating the process to achieve a dense pore free layer is required -Precursors are expensive
Tape casting	Inexpensive and effective	Geometric restrictions
Tape calendaring		
Screen printing		
Dip coating	-Most convenient for tubular SOFC -Simple -Non-expensive	Problems with repeatability

One way of applying an evenly distributed membrane layer on top of a substrate is by dip coating. This involves immersing the substrate in to a solution with dispersed electrolyte material. This is the chosen method for this thesis since it is relatively simple and inexpensive. For creating the solution used for dip coating a combination of YSZ powder, solvent and binder are mixed. Sometimes a disperser and/or plasticizer are incorporated as well. Manual stirring, ball-milling and ultra-sonication can be used to blend and homogenize the solution. Various recipes for the dip coating has been created by different research groups and common chemicals used for these and their ratios are depicted in Table 6 below. It can be seen that there are many different ways to create these solutions which indicate the simplicity of this method. There is also a variation in the dipping speed, soaking time as well as how many times this procedure is repeated.

Table 6. Various recipes for dip coating solutions used to create a dense electrolyte layer [30] [31] [43] [44] [45].

	Chemicals	Common recipe proportions				
Powder	YSZ	9	10	15	16	10
Solvent	Ethanol	90	100	-	27	86
	Butanone	-	-	-	54	-
	2-propanal	-	-	35	-	-
	Terpineol	2.4	-	-	-	4.2
	Toluene	-	-	21	-	-
Binder	Ethyl cellulose	0.15	-	-	-	0.27
	Poly ethylene	-	0.15	-	-	-
	Poly vinyl butylene	-	0.30	2.0	1.5	-
	Poly ethylene glycol	-	-	-	0.50	-
Disperser	Triethanolamine	-	-	-	0.50	-
	Triton X-100	-	-	0.30	-	-
	Sorbitan trioleate	-	-	0.15	-	-
	Corn oil	0.45	-	-	-	-
Plasticizer	Di-n-butyl phthalate	-	-	1.5	0.50	-

2.3 Characterization

2.3.1 Optical microscope

An OM works by magnifying light, which has interacted with the sample, with the use of lenses. An OM with good lenses can reach magnifications up to X250. This upper limit is caused by the wavelength of light which is around 0.5 μm. With minimum aberration the resolution achieved can be 0.3 μm. When using opaque samples the light is reflected off from the surface. As the magnification increases the spatial distance between the sample and the microscope decreases which can be observed as a reduction in light intensity. Thus at higher magnifications a good light source is needed to illuminate the sample. Also at higher magnifications the depth of focus becomes smaller, which makes highly topographical samples look rather nebulous [46].

2.3.2 Scanning Electron Microscope

SEM is a characterization tool used to achieve high-resolution images of a sample. Its maximum magnification is superior to the OM since it uses electrons as a beam, and is thus not limited by the wavelength but by aberrations in the microscope. The electrons are emitted from what is called an electron gun and reaches the sample with a very high energy after going through a series of apertures and magnetic lenses. The electron ray is precision scanned on top of the surface to generate signals which are used to create an image. At the sample the electrons will interact in different ways. When constructing an image the two most common interactions used are backscattered electrons (BSE) and the production of secondary electrons (SE) [46].

SE can be formed when an incident electron knocks out an electron from one of the atoms of the sample, see Figure 5 b). These electrons have low energy and cannot travel very far in the sample, typically less than 2 nm, which means that those SE that escape the sample are generated from a very thin layer on the surface, see Figure 5 a). This allows topographical contrast to occur since more SE can be emitted on edges than on flat surfaces [46].

BSE are in essence the electron beam being affected by the atoms in the sample in such a way that it changes direction completely and scatters out from the sample (Rutherford scattering), see Figure 5 c). The BSE can be used to visualize the difference in chemistry of the sample, especially if there are great differences in the atomic number between the elements. This is because the higher the atomic number (more protons) of an element the greater the attraction force to an electron, which increases the probability to sling shot the electron away. The heavier elements thus appear brighter than the lighter ones. This is however especially true if the structure and density is uniform [47].

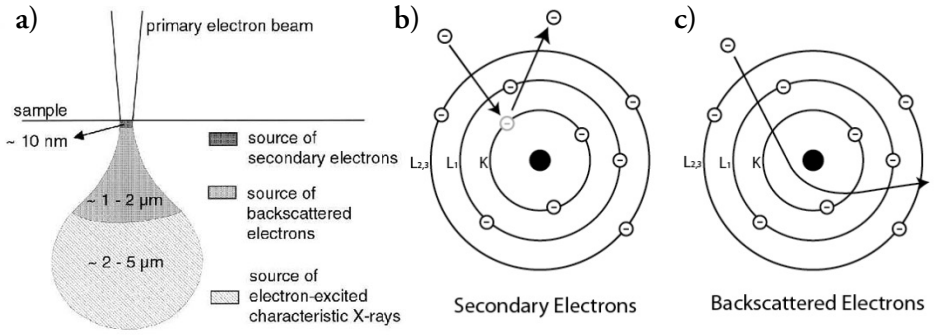

Figure 5. a) The excitation volume showing how deep common interactions can take place. The mechanisms behind SE and BSE formation in b) and c) respectively [48] [49].

2.3.3 Energy Dispersive Spectroscopy

According to the Bohr atomic model the electrons in an atom is occupied in different shells. Depending on the weight of the atom it will have a different amount of shells, named K, L, M etc., with K being closest to the nucleus. Each shell has its own specific energy, with K having the largest. As stated in the section above, SE are electrons that has been ejected from a sample atom, which can happen for any of the shells. If this occurs to an electron in the K-shell of an atom, say nickel which has a K, L, M and N-shell, an electron from either the L or M-shell will lower its energy and move down to the K-shell. For this to happen the electron sends out energy in the form of an x-ray which will have the same energy as the difference between the two shells. Similarly an electron from the L-shell (or M-shell for the heavier elements) can be knocked out which is seen in the spectra as an L-peak and M-peak respectively. Since each element have unique shell energies they will produce characteristic x-rays and a distinction can thus be made between them. Peak overlaps can however occur, especially for elements with similar atomic weights or elements were K-peaks overlaps with L-peaks. This can make the distinction more challenging but there are some tricks that can be used. For the K-shell x-ray interaction, 1 in 11 generated x-rays will be from the M-shell and the rest is from the L-shell. This is seen in the spectrum as two peaks close to each other, with one having

tenth the size of the other. The same proportion does not occur for the L-peaks. Looking at both the L-peaks and K-peaks of an element can be used to see if the element exist in the sample. Since the x-rays are generated from relatively deep within the sample, see Figure 5 a), confusion can occur when looking at μm thin samples. Also when looking from above at samples with thin coatings the chemical information of the underlying material can show up in the spectra [47].

3 Experimental

The experimental part essentially comprises five steps; substrate formation, nickel impregnation, AFL application, electrolyte application and cathode application. Below is shown how the ceramic fibre paper changes during the course of the different application methods.

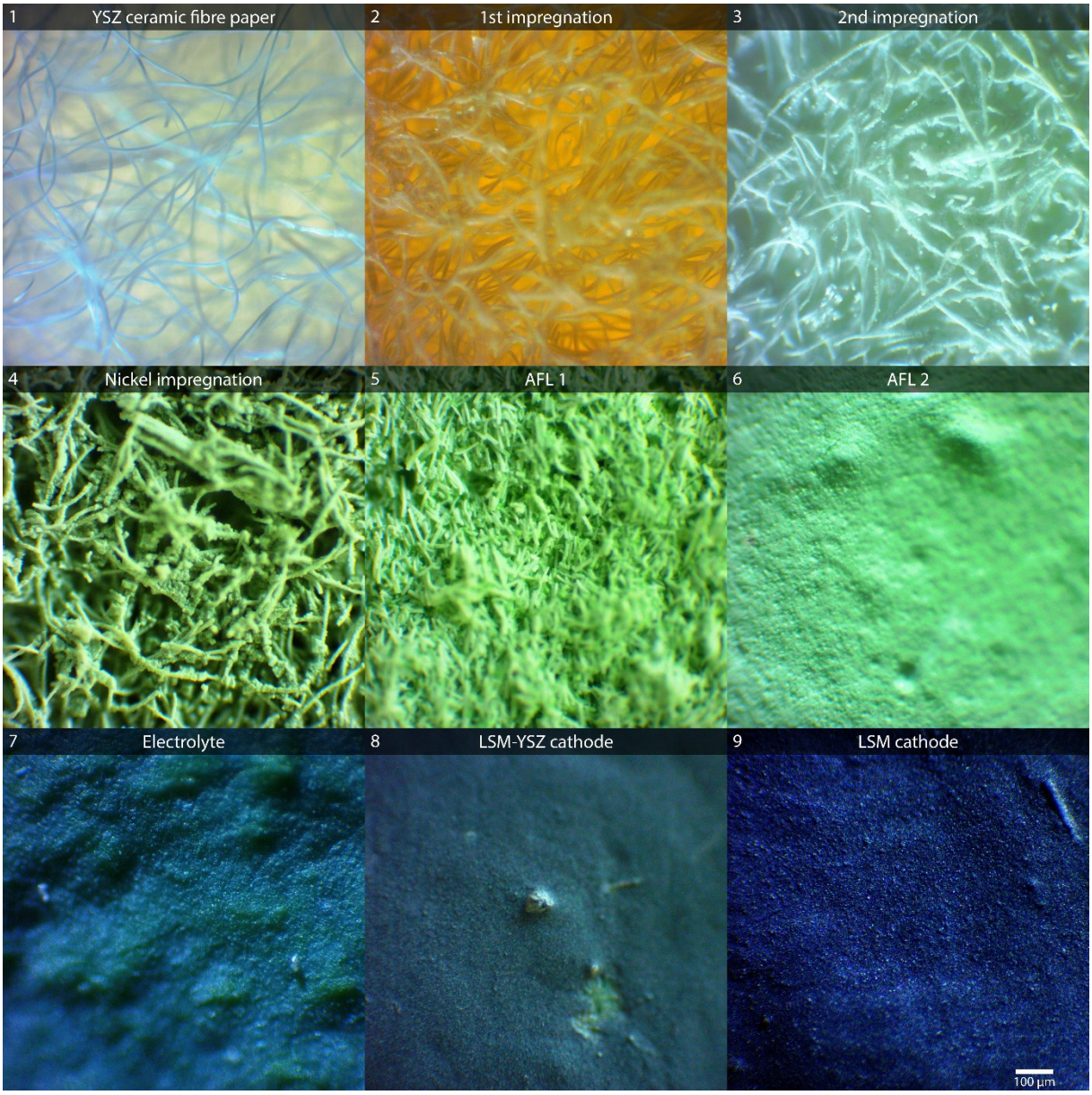

Figure 6. A X10 magnified view of how a ceramic fibre paper evolves in to a SOFC unit.

3.1 Materials

The most commonly used chemicals in this thesis are YSZ colloidal solution, YSZ powder, NiO powder, ethyl cellulose, terpineol and ethanol. A more detailed list of the different chemicals and other materials used is given in Appendix B.

3.2 Laboratory work

In this section the experimental part of this thesis will be detailed. Different setups were performed and parameters have been changed during the course of the project. Only the last setup will be described here but a discussion on developing the setup will take place in section 4.1. The different experimental steps are summarized below. Every step is followed by drying and calcination at different temperatures and times. A total of three different ovens were used.

3.2.1 Substrate formation

Since a lot of different parameters had to be tested, planar substrates were constructed since they are easier to produce than tubular. However tubular samples were made towards the end of the project. The sizes were 20x20 mm for the planar and 50x10 mm for the tubular.

YSZ fibre papers with a thickness of around 1 mm were cut in to the appropriate sizes followed by impregnation. A mixture of yttria and zirconia colloidal solutions were blended to create an 8 mol% yttria solution to be used for the impregnation, for calculations see Appendix A1. A water aspirator utilizing the Venturi effect was used to create a vacuum in order to vacuum pressure impregnate the samples.

To create the flat substrates two or three impregnated papers were pressed between two aluminium sheets using screws and bolts. For creating the spacing, rings with different thickness were placed around the screws in between the metal sheets. The surface of the sheets were sprayed with Vaseline® to prevent the papers to stick onto the metal during drying. The thicknesses investigated were 1, 1.5 and 2 mm. In Figure 7 to the right a setup using two 1mm rings to create a 2mm pressing can be seen. The samples used for this image are 10x10mm and used in the early setups but the principle is the same.

Figure 7. Early setup to create 2 mm thick samples.

A basic cylindrical shape was achieved by using a pipe and a tube as mould. The tube was cut in half trough the diameter to create two pieces. An impregnated fibre paper was rolled around the pipe and then squeezed between the two tube pieces with the aid of two clip ties. The tube had an inner diameter of 10 mm and a length of 50 mm. Since it was sawed using a hacksaw with a 1mm blade it became slightly oval shaped. The different thicknesses were achieved by using pipes with varying outer diameter, see Figure 8 below.

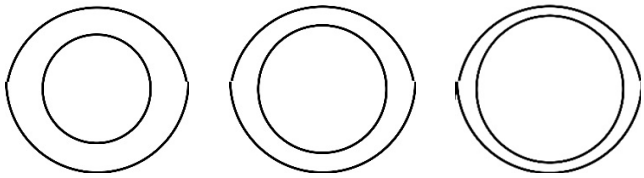

Figure 8. Basic cylindrical shapes seen from the rear end, illustrating the thickness variations achieved for the tubular samples.

The impregnated ceramic papers were first heated up to 120 °C and were kept 4 h at each of the following temperatures: 80 °C, 90 °C, 100 °C and 120 °C. This was done since the aluminium press created a very narrow space in which the water could evaporate from, and thus took a long time. Also, keeping the temperature below 100 °C inhibits the boiling of water which could cause structural deformation to the samples. After this the samples were loosened and calcinated at 950 °C for 4 h. The heating and cooling rates were the default values, typically a couple of hours, for the ovens used (Nabertherm®, model L3/11/S27, with a maximum temperature of 1100 °C). This oven was also used for the heat treatment of the nickel impregnation and the AFL application.

The samples were vacuum pressure impregnated once again, either with a YSZ or ceria colloidal solution. After the first impregnation the samples became rigid so no pressing was needed the second time. The drying and calcination scheme for the second impregnation was the same as the first one except that it stayed 30 min at the given temperatures during the drying procedure. How the microstructure changes during these steps can be seen in Figure 9 below.

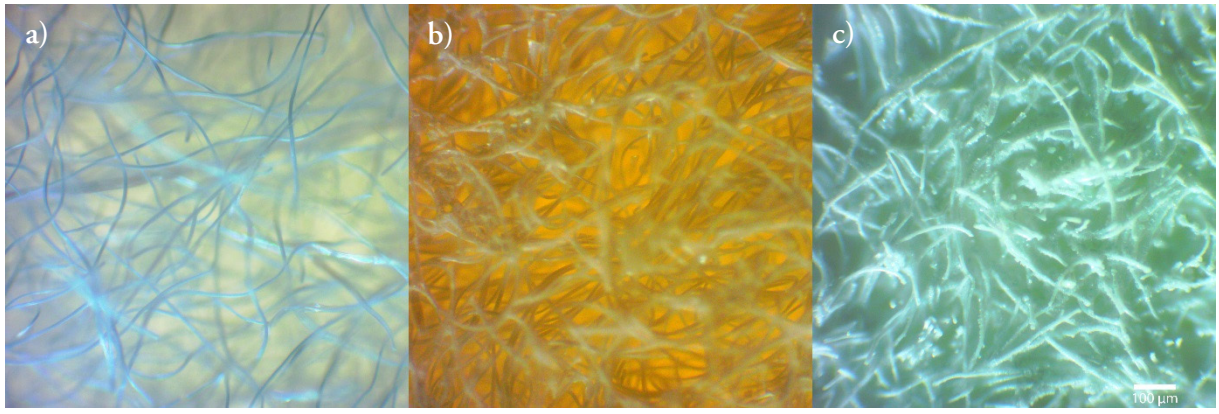

Figure 9. The microstructural formation for the colloidal solution impregnations showed at X10 magnification with the YSZ fibre paper depicted in a), first impregnation in b) and second impregnation in c).

3.2.2 Nickel impregnation

In order to make the anode catalytic and electrically conductive, nickel was incorporated as $Ni(NO_3)_2*6H_2O$ into the substrate by vacuum pressure impregnation. The fact that $Ni(NO_3)_2*6H_2O$ decomposed to NiO, see Formula 3 below, had to be taken in to account when mixing the solution since the weight decreases significantly. A solution of $Ni(NO_3)_2*6H_2O$ and H_2O was made so it corresponded to a 17 wt% NiO solution, see Appendix A2 for calculations. The drying and calcination were done by heating the samples to 950 °C for 4 h via the temperatures 80 °C, 100 °C and 120 °C and staying at each for 30 min to allow evaporation of water. The heating and cooling rates were the default values for the oven used, typically a couple of hours. The microstructure can be seen in Figure 10 to the right.

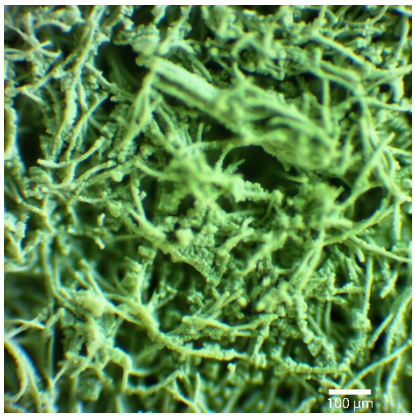

Figure 10. The microstructure after nickel impregnation.

$$2\mathrm{Ni(NO_3)_2} * 6\mathrm{H_2O} \rightarrow 2NiO + 4\,NO_2 + O_2 \quad (3)$$

3.2.3 Anode Functional Layer

In order to get a smooth surface for the electrolyte application a layer on top of the anode substrate was made, the AFL. This was done by making a paste and applying it on top of the substrate using a paintbrush. For the creation of an even and crack free AFL, different pastes were manufactured by varying the proportions of the ingredients.

The AFL consists of two different consecutive layers, denoted here as AFL1 and AFL2. Both consists of powders, binders and solvent but AFL1 also contain YSZ-fibres as to make the transition from the fibre substrate smoother. A specific ingredient list for these are given in Appendix C. The paste for AFL1 was manually mixed and ultra-sonicated for 1h, while AFL2 was ball-milled for 100h and ultra-sonicated 1h before use. A Branson 200 ultrasonic device and a homemade ball-mill were used.

The powders used for AFL1 was either NiO or a mixture of YSZ and NiO to see if there would be any difference in crack development or bending due to the different TEC.

Both AFL1 and AFL2 was applied thinly mainly to avoid a too thick AFL which might increase the chance of crack development. However the AFL2 was too thin and did not completely cover the YSZ fibres. A second AFL2 was therefore applied. Even after this second layer there were samples with small holes in them or other discrepancies. These samples were painted again either entirely or partially.

The drying and calcination of both layers were completed at 950 °C for 4 h with a stay at 220 °C for 2h. This was done since the main solvent, terpineol, evaporates around 230°C. The heating and cooling rate were set at 1.5 °C/min.

A X10 magnification of how the AFL looks like can be seen in Figure 11 below.

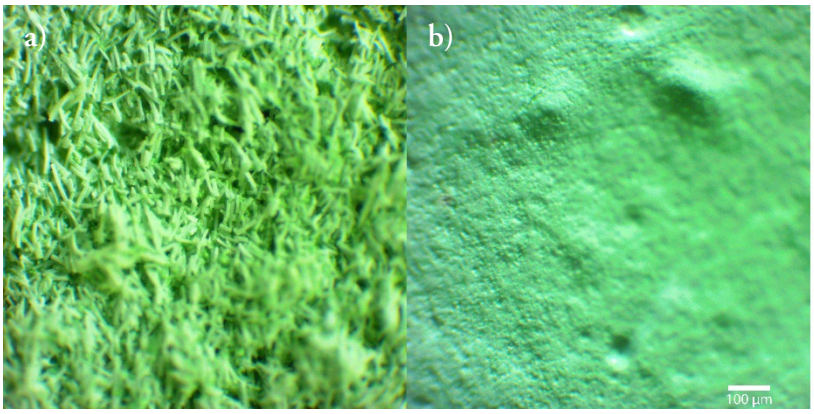

Figure 11. Close up on a) AFL1 and b) AFL2.

3.2.4 Electrolyte

Dipping and dripping were used for tubular and flat samples respectively when applying the electrolyte layer. For a recipe of the electrolyte solution used, see Appendix C.

A glass Pasteur pipette was used to drop the electrolyte fluid on top of the samples. The low viscous fluid formed a thick non-uniform layer on top of the samples which was distributed as evenly as possible by tilting the samples in various ways for several minutes. Around 20 drops were used on all samples and some were reapplied with 10 drops 1 hour later due to uneven or a seemingly too thin layer. The samples were then left to dry for 24 h in a fume hood. After this procedure the samples were sintered in a tube furnace at 1400 °C for 4 h with a heating and cooling rate of 1 °C/min. The furnace used was a Lenton Furnaces, serial number 4202, with a maximum temperature of 1500 °C.

After the sintering, some samples needed a reapplication of the electrolyte due to microscopic crack development. These were applied with 10 drops of the solution and given the same drying and sintering scheme as before.

The tubular samples were slowly dipped into the solution, emerged and then slowly withdrawn. All these three steps were done for approximately 10 seconds each. They were allowed to dry for 48 h in a fume hood and treated with the same furnace program as the planar samples.

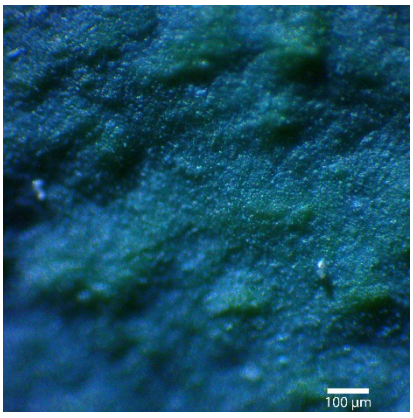

Figur 12. Electrolyte layer

The electrolyte application is depicted at X10 in Figure 12.

3.2.5 Cathode

For the application of the cathode, two layers were applied; one containing a 50:50 mix of LSM:YSZ and the other consisting of pure LSM. Using a 50:50 blend increases the TPB and an LSM layer on top of that increases the electrical conductivity. These are shown in Figure 13 below.

The cathode ink supplied by NexTech Materials has been stored at Catator for several years and its constituents had slightly segregated. To resurrect the ink it was manually stirred for a couple of minutes and ultra-sonicated for 1h. Both cathode inks were applied as thinly as possible using a paintbrush. The electrolyte wasn't applied all the way out to the edges, about a millimetre frame was left unpainted to ensure that no short circuits would arise from the cathode touching the anode at the edges. After application the samples were left in a fume hood for 1 h until the surface was no longer looking dark and wet. The samples were later calcinated at 1100 °C for 4 h with a heating rate of 2 °C/min to 500 °C and 3 °C/min to 1100 °C with a cooling rate of 3 °C/min. The oven used was a Nabertherm®, model HO 70, with a maximum temperature of 1280 °C.

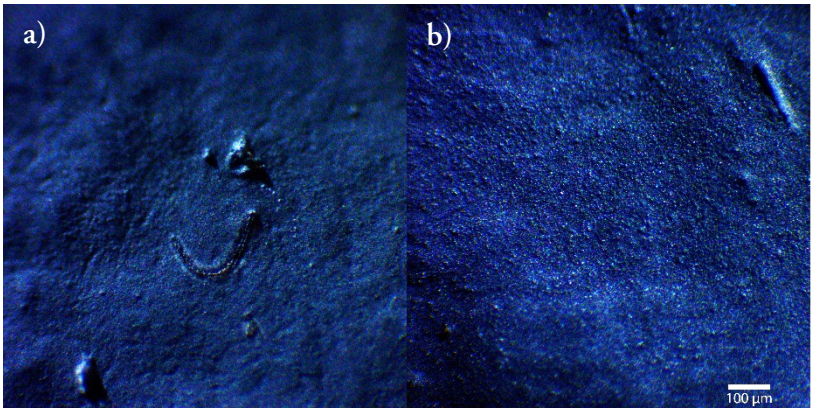

Figure 13. The a) LSM-YSZ and b) LSM cathode layers depicted at X10 magnification.

3.3 SEM and EDS

Three SEM sessions have been conducted in order to get a magnified understanding of the produced samples. An EDS analysis was simultaneously conducted at the SEM sessions for knowledge about the chemical composition. Prior to the SEM operation the samples were coated with a thin layer of carbon using a Balzers CED 030 Carbon Evaporator. This was done to increase the conductivity of the samples and thus producing higher quality images.

3.4 Performance test

In order to evaluate if the planar samples were working, a performance test was made by constructing a test oven from a steel tube with a diameter of 50 mm. The tube was coiled by a kanthal wire that was used as a heating element due to its high electrical resistance and high heat resistance. A tailored fuel cell holder was constructed and placed inside the tube which was later isolated, see Figure 14 below. In the figure the fuel cell (green) is constrained by the fuel cell holder which consists of two chambers. The one to the left, which has larger window holes, is the cathode

side and contain air. The right chamber (which in reality didn't have any small holes in the walls) is the anode side and contains a H_2/N_2-atmosphere. The gases in these two chambers should not be mixed in order for the evaluation to work as they could react with each and thus prevent the ion and electron transport to take place. The fuel cell holder also act as a conductor for the electrons produced at the anode, guiding them out of the oven via a voltmeter and back in again to the cathode which enables a verification of the sample function.

A sample was put in to the fuel cell holder and applied with conducting silver paste. This paste would ideally also create a gas insulation as to prevent the two gases to mix but since this wasn't the case the chamber needed to be insulated in another way. This was done by making a paste of powder, fibre and colloidal solution consisting of YSZ. This paste was put on the edges of the fuel cell as well as on the two chambers. After this the test tube oven was put on top of the arrangement and insulated.

The oven was supposed to be heated to 750 °C but malfunctions in the system caused the heating process to shut down around 500 °C.

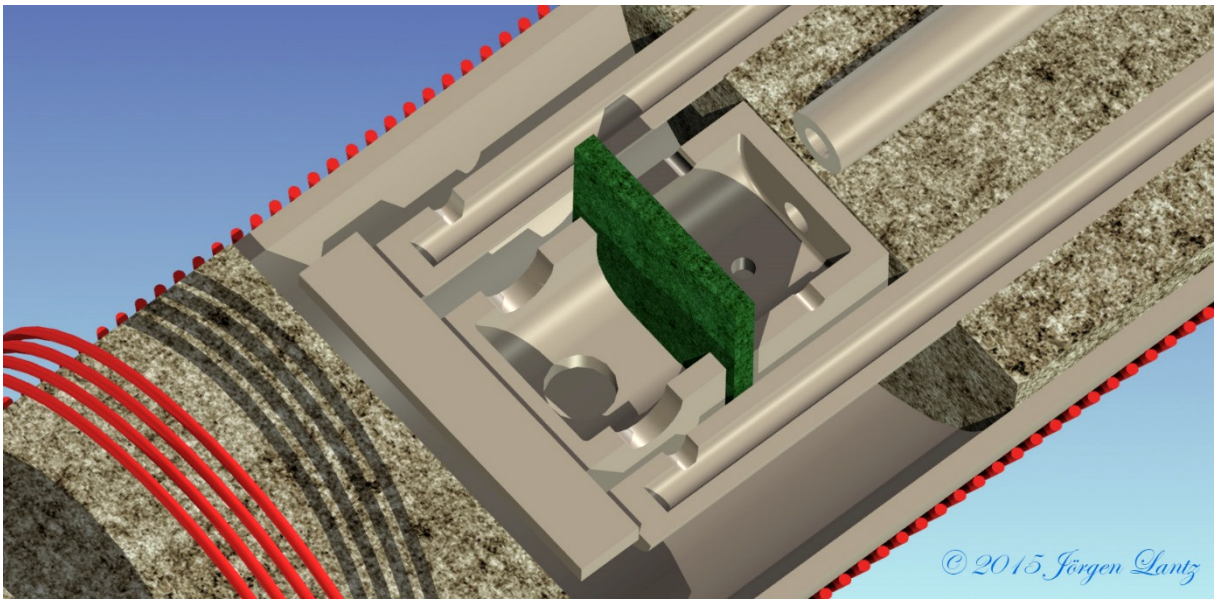

Figure 14. Test oven setup showing the fuel cell holder inside an insulated tube surrounded by wires which heat the system.

4 Results and discussion

4.1 Experimental

In this section various results and thoughts from the experimental part will be discussed.

4.1.1 Substrate formation

Different approaches regarding colloidal solutions were followed in order to achieve a rigid substrate. In the beginning an alumina colloidal solution was used which resulted in a less homogeneous crystallization behaviour than the YSZ colloidal solution. This was especially true for the corners and edges of the samples. For the second impregnation no conclusion could be drawn as to whether the YSZ or ceria solution was the better option. During the tube formation, it was rather difficult to achieve a round cylinder shape due to the rolling and pressing which resulted in various shapes. In Figure 15 a) a 2mm thick tubular sample is depicted, it can be seen were the two half-tube moulds have been pressing and deforming the sample. In b) a more uniform sample is presented.

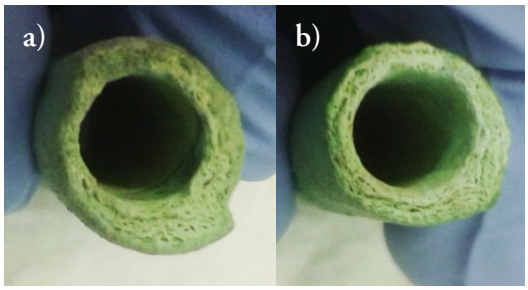

Figure 15. Two different 2mm tubular samples showing the importance of manufacturing technique.

4.1.2 Nickel impregnation

Different nickel solutions were made, consisting of both NiO powder and $Ni(NO_3)_2*6H_2O$. The NiO-powder solution was proven to be difficult to deal with due to several factors. The solution was very opaque which caused the samples to seemingly disappear into the liquid during the impregnation. Due to this reason, several samples broke when using a metal tweezer to pick them up after the impregnation. Due to sedimentation of the powder there was an uneven distribution on to the samples as they sank to the bottom and collected powder on the side laying on the bottom of the beaker. This in turn made it difficult to pre-estimate the weight gain of NiO and develop a consistent method. However these samples showed less bending but more cracks.

It has been reported that the nickel nitrate could be added after the cathode, followed by drying and calcination at 950 °C [21]. This will lower the coarseness of the nickel particles in the anode since they will not be subjected to the electrolyte sintering temperature. However the application method should be one that does not immerse the sample in to a solution as to hinder any coating of the cathode and membrane. Especially not to create a short circuit between the anode and

cathode. The samples could however be polished at the edges to remove any conductive material connecting the anode and cathode.

Some groups have been using a 5M $Ni(NO_3)_2$ solution to impregnate a porous YSZ matrix. They achieved a nickel distribution of 10 vol% after several impregnation cycles [50]. The distribution achieved in this project after 1 impregnation of a 2 M solution was around 6 vol%, see Appendix A2.2 and A3 for calculations. This indicates that the samples in this project have a much greater porosity, but whether this is beneficial or not, with regard to the electrical conductivity, cannot be known without any tests done so it is hard to say if this value is enough or not.

In Figure 16 below the nickel distribution within the substrate is depicted for different setups, a more descriptive image of these, including spectra, can be seen in Appendix D. These distributions are not satisfying since there should be a connected network in order to achieve sufficient electron conduction. The different solutions used to impregnate the samples are shown in the Table 7 below. Unfortunately the nickel impregnation performed as 2M nitrate solution was done after the SEM sessions had been conducted and a distribution image can therefore not be presented for these. It is however shown in the table as a comparison and would most likely give a more satisfying distribution.

It should be noted that some x-ray signals are physically blocked creating a shadowing effect observed in some images. This is due to topographical differences.

Table 7. The different solutions used to impregnate samples shown in the EDS image below.

Denoted in figure as	NiO / g	$Ni(NO_3)_2*6H_2O$ / g	Water / g	Ethanol /ml	Triton X-100 /drops
a)	4.2	-	-	50	-
b) and c)	23	22	150	-	100
2M sample (not in figure)	-	62	78.2	-	-

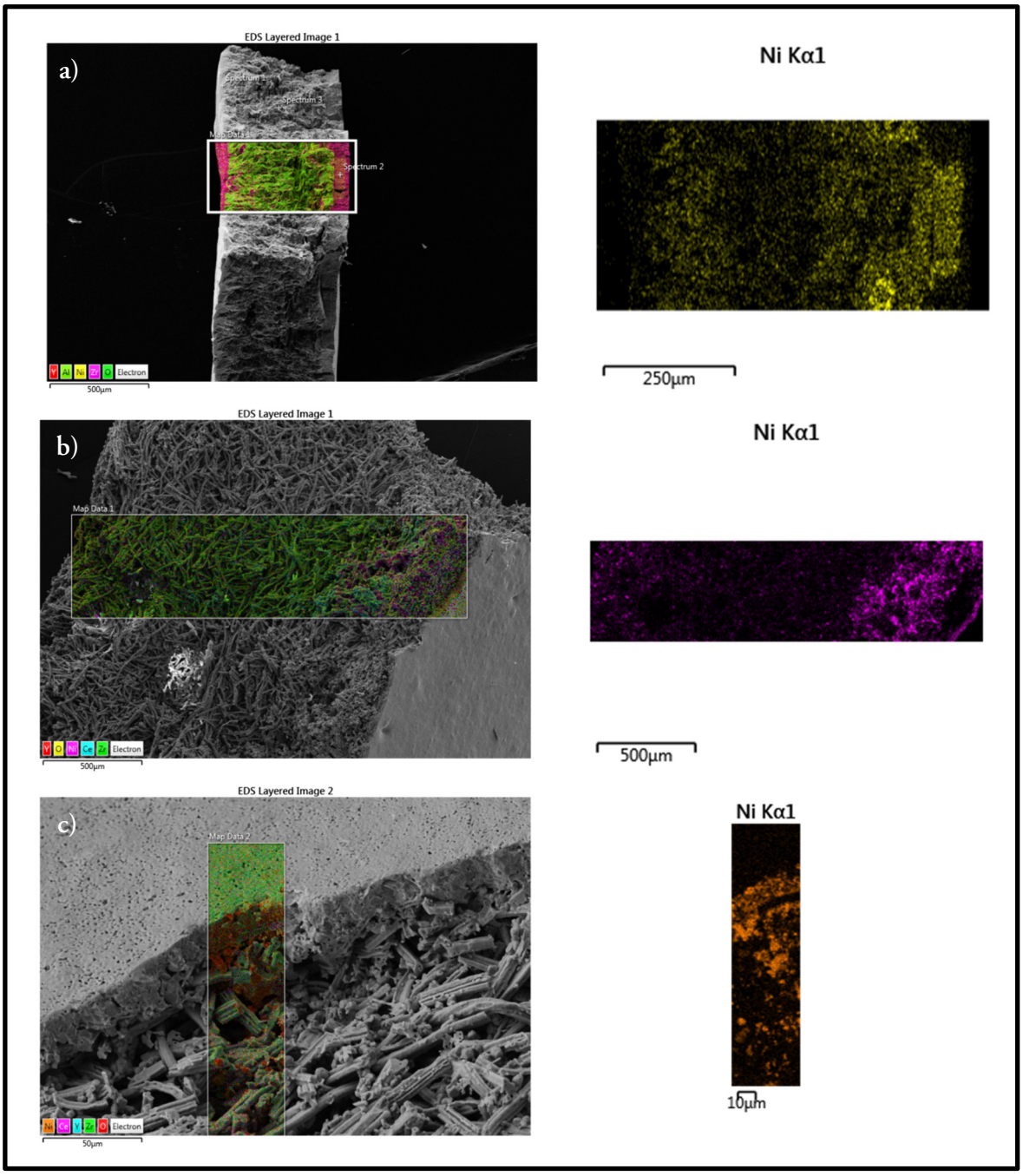

Figure 16. EDS images showing the nickel distribution for different samples. The images to the left has been map scanned and their corresponding nickel map is shown to the right. The magnifications are X50 for a) and b) and X500 for c).

4.1.3 AFL application

The AFL1 application appeared to have a smoother surface when it was applied as a rather thick layer while for some samples the AFL2 showed the best result when it was applied as a thin layer. However some other samples needed a thicker AFL2 in order to completely cover the fibres of the AFL1. Usually the thickness of AFL1 is greater than AFL2 since some of it gets sucked up in the fibrous network. For the last samples the AFL1 comprised 60 % of the total AFL.

It would have been good to make the AFL pastes more homogeneous since it had problems with some grains being too coarse which cause thickness differences of the electrolyte layer which in turn makes it less durable.

Both NiO and NiO-YSZ powders were used in the AFL1. The conclusion drawn from this was that the NiO based AFL1 showed less bending, see Figure 17 below. The ones in column 1 and 2 contain NiO-YSZ while 3 and 4 contains NiO. Rows 2, 4 and 6 has been impregnated with ceria during the second impregnation but no real distinction in physical appearance can be drawn between them. A slight difference between the thicknesses can however be observed. The two top rows are 1 mm samples and the bottom 2 rows are 2 mm samples. The thinner samples tend to be a bit more shaped.

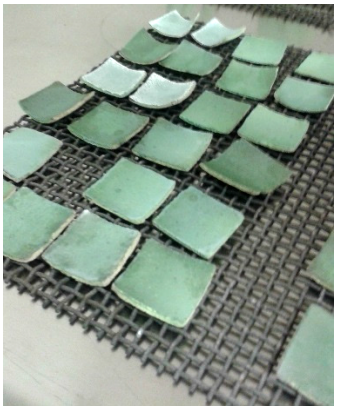

Figure 17. Image showing the bended appearance after the electrolyte sintering.

A paste was made that contained NiO-GDC instead of NiO-YSZ. Since GDC has higher ionic and electrical conduction this was predicted to give a better performance of the cell. However these samples were more prone to form cracks and thus eliminated from the procedure.

Figure 18 below shows a sample of an alumina fibre paper of which the applied surface layers had cracked open during sintering, probably due to differences in TEC. The green layer is most likely the AFL2 and electrolyte layer while the blue and white looks like the AFL1 with traces of the fibrous substrate. The thickness of the green layer is around 40 μm.

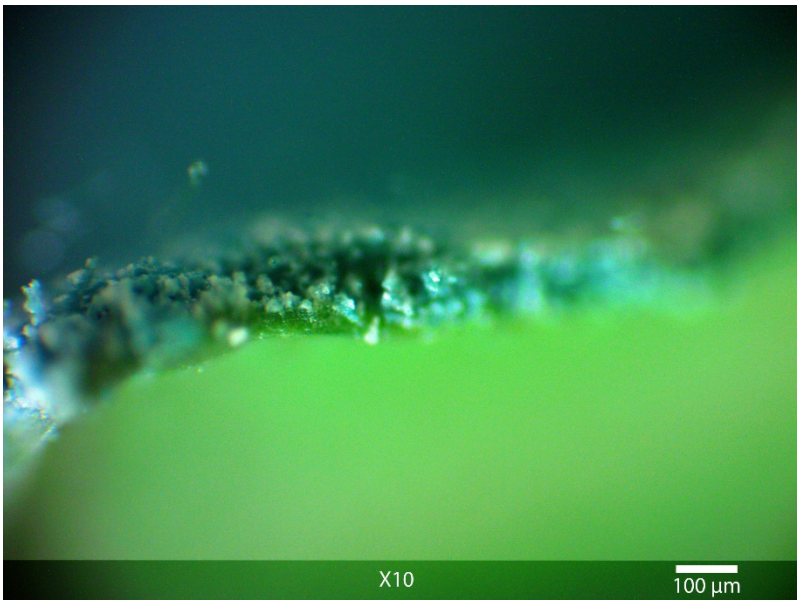

Figure 18. A cracked open alumina fibre paper sample showing the thickness of the AFL and electrolyte layer.

4.1.4 Electrolyte application

This sections will cover how the samples appeared after the electrolyte application and heat treatments at 1400 °C which includes the properties of the electrolyte and the appearance of the samples.

While the alumina paper was much easier to shape and handle than the YSZ paper the smaller samples often flaked while larger samples frequently cracked during the electrolyte sintering. This can be seen in Figure 19 and 20 in normal scale and at X10 magnification respectively. Due to this reason the alumina paper was eliminated from the experimental process.

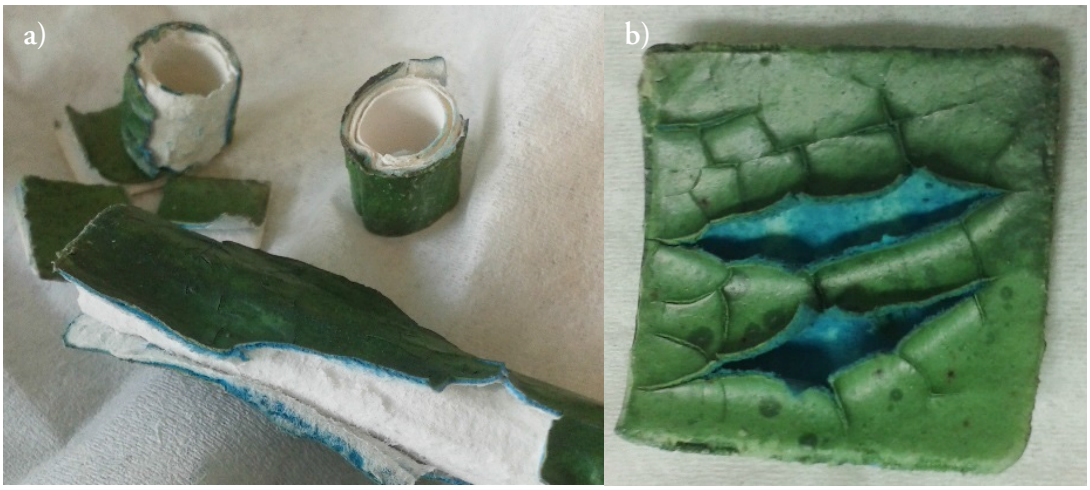

Figure 19. Cracked a) tubular and b) planar alumina paper samples as they appeared after the electrolyte sintering.

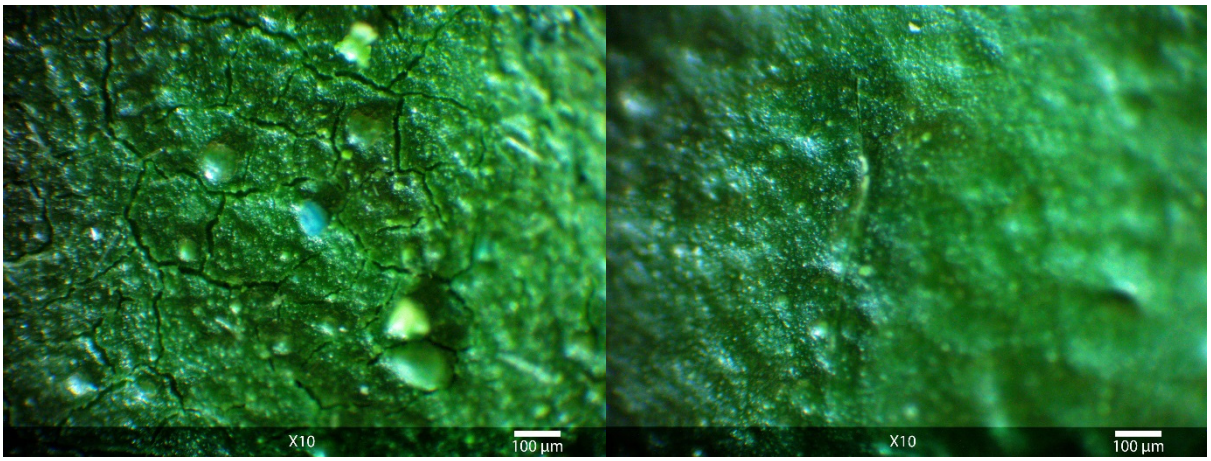

Figure 20. The influence of substrate material on the applied layers is illustrated at 10X magnification. Alumina paper to the left and YSZ on the right. The experimental methods are the same in both cases.

When the samples were taken out of the tube oven the majority had bent in a concave manner, probably due to the difference in TEC and the shrinkage of the electrolyte layer, see image below.

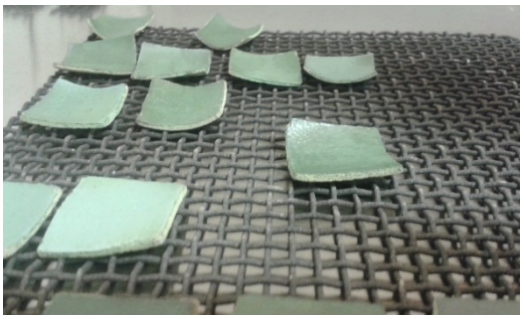

Figure 21. Image depicting the bending behaviour of samples.

The samples that were examined with the SEM were coated with the dip coating technique. This was however switched to a drip and tilt method as described in section 3.1.4 since the electrolyte solution could cause YSZ particles to partially block the nickel phase which might lower the performance.

In Figure 22 below various SEM images are depicted showing the surface of three different setups. A brief description of these are seen in Table 8. The sample depicted in a) can be seen to contain very large ruptures but showed a better electrolyte densification which is probably due to the greater number of repetitive coatings. At the time the cracks were thought to be due to the amount of coatings. However it is most likely due to the alumina paper having a different TEC. In some of the images below the electrolyte layer can be seen as well as the underlying fibrous network. The electrolyte layer is around 15-20 µm thin for the sample in b) while it is around 30 µm for the sample in c). Based on the small pin-holes, a semi-dense membrane is produced for all samples. In the left image of c) the electrolyte, the part that is not blurry, seems quite dense but when looking at the right image however the surface isn't quite so dense, it also shows crack formation. It should be noted that all examined samples had cracks and irregularities of some form.

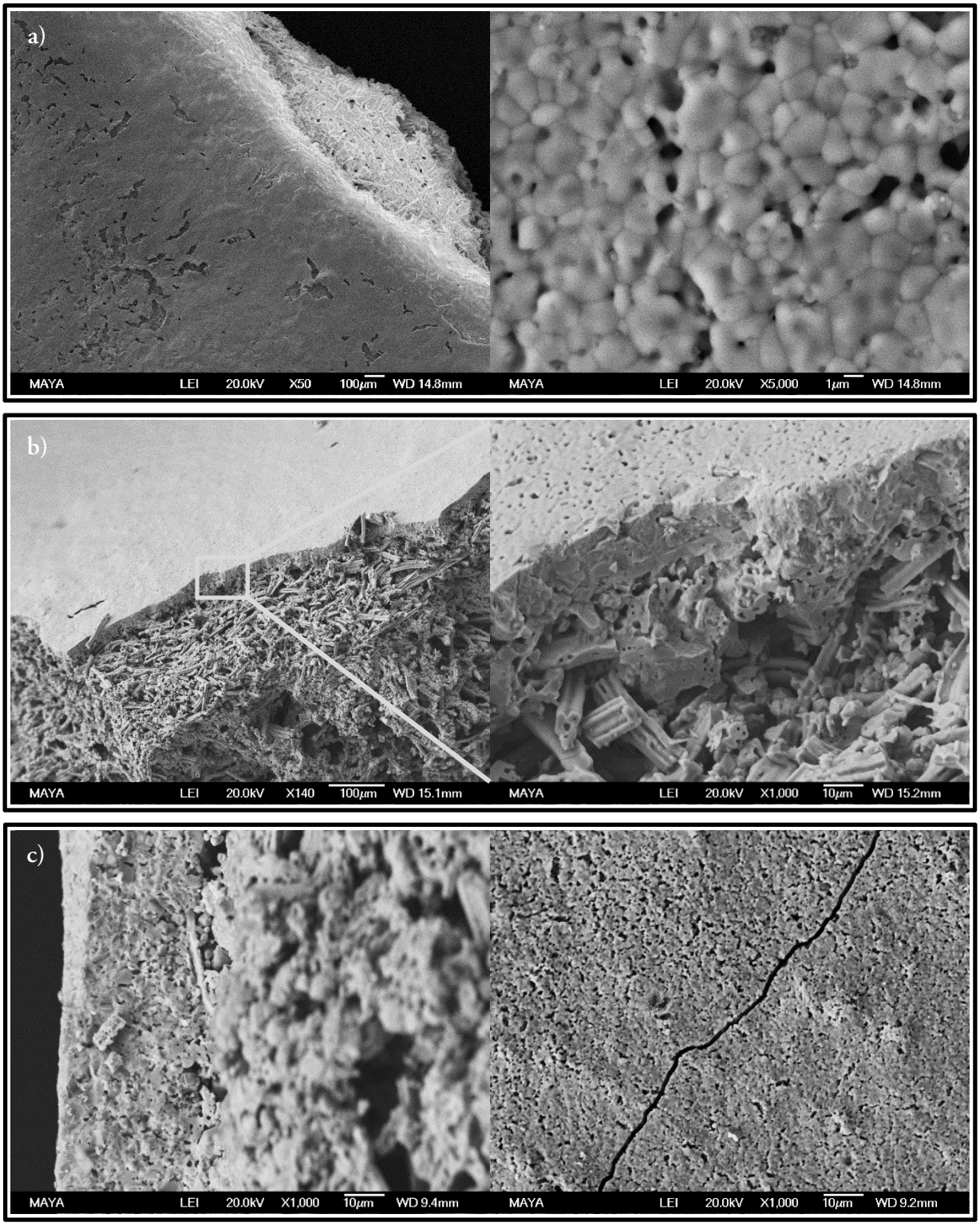

Figure 22. SEM images of three different setups which are depicted in a), b) and c). See Table 8 for their manufacture specs.

Table 8. Manufacturing information for the images shown in Figure 22 on the previous page.

Sample	Paper	Imp1	Imp2	AFL1	AFL2	Electrolyte
a)	Alumina	Alumina	Alumina	NiO-YSZ fibre	-	10x dip
b)	YSZ	YSZ	Ceria	GDC-YSZ fibre	Regular recipe	1x dip
c)	YSZ	YSZ	YSZ	NiO-YSZ fibre 2 thin layers	Regular recipe 2 thin layers	(1x dip) x2 sintered twice

The tube samples had small cracks visible to the naked eye. One of the 1 mm samples had a rupture half way through were the tube moulds were pressing, see Figure 23 a). Another 1 mm sample showed an oval formation, Figure 23 b).

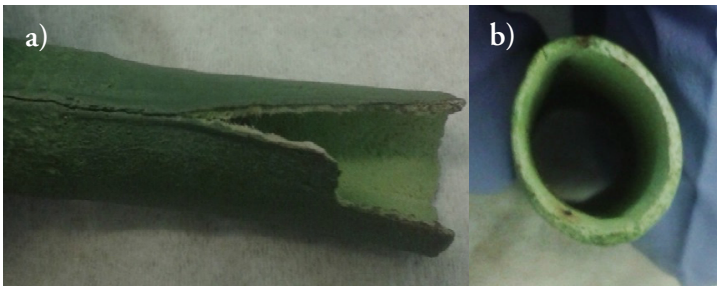

Figure 23. Faults generated to 1 mm tube samples after electrolyte sintering.

The tubes had a rougher surface than the planar and needed to be coated with more AFL in order to make the surface smoother. When they were made the paper was rolled on to a pipe and then pressed. During the pressing there could have been forces acting on the paper in such a way that crevices formed, thus making it rough. The extra thick AFL layer probably caused more tension to be formed due to different TECs. It was also observed that the tubes had decreased significantly in size and upon measuring the length had decreased 10 %. The cracks could thus also have originated from tensions during the densification of the electrolyte.

4.2 Weight measurements

A comparison between the different steps was made with respect to the increase in weight. Four planar samples of each thickness were weighed along the course of the experimentation and a mean value was calculated for these, see Figure 24 below. The image shows the added weight as a relative value to the non-treated fibre paper. The last step of adding the cathode was not taken into account since most samples were bent and adding this layer seemed unnecessary. The 1.5 mm samples showed the most relative increase for the three impregnation steps. This is because the 2 mm samples used three stacked papers and the others used two papers. The 1.5 mm sample thus has the highest porosity and therefore a higher capacity for absorbing liquid.

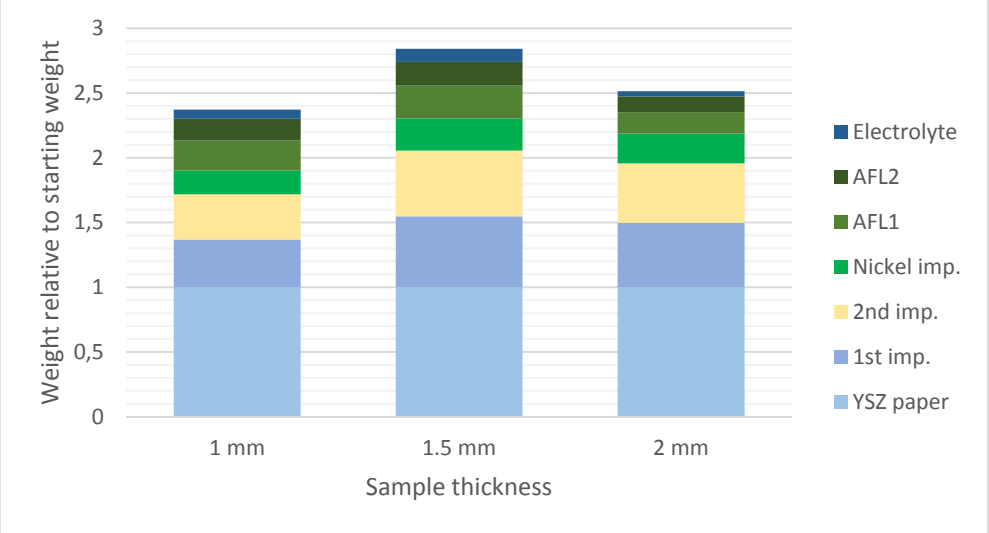

Figure 24. Weight increase of the different steps relative to their starting weight.

The tubular samples were weighed after the electrolyte application. The samples with the least amount of damage, i.e. cracks and physical deformation, was the 1.5 and 2 mm samples. Their weights were compared to a conventional SOFC used by Catator in previous testing for the same application and turned out to be 50-60 % lighter. These were SOFCs without the cathode layer but it is estimated that the weight is around half of the conventional one. It should be noted however that these samples probably wouldn't work since there were too many cracks in the surface.

4.3 Performance test

There was only one planar sample that was flat enough in order to fit satisfyingly inside the fuel cell holder. All the other samples were bent in such ways that they created too large patches between the fuel cell and the holder. This made it too difficult to create a conducting layer in between the chambers and the sample. This was especially true between the cathode side and the air chamber since only the edges of the sample touched the chamber which required extra paste at the closest corner, see Figure 25 to the right. The test oven didn't go through with the heating program and shut down automatically at around 500 °C. This occurred three times and is believed to be caused by short circuits probably due to defects in the ceramic insulation of the test oven. Since there was no more time to do any further tests the functionality of the SOFC produced will remain unknown.

Figure 25. Setting up a sample before testing.

5 Conclusion

A light weighted SOFC has been manufactured utilizing a ceramic fibre paper as a backbone structure. An alumina and YSZ fibre paper were compared and the alumina was discarded due to high levels of crack development. The flexible fibre paper has been shaped into flat and tubular formations followed by vacuum pressure impregnation using colloidal solutions. Two consecutive impregnations were done using YSZ and YSZ or ceria solutions in order to achieve a rigid structure. No conclusion can be drawn whether or not the second impregnation is better to do with YSZ or ceria. Nickel was incorporated in to the structure as oxide powder and or nitrate salt solution in order to make the anode electrically conductive and catalytically active. The nitrate salt solution was a better choice since sedimentation of the NiO powders caused unreliable distributions onto the samples. The substrate was too porous in order for an electrolyte layer to be applied on top of it so a smooth less porous layer, the AFL, was applied on top of it. This layer was divided in to two sections, AFL1 and AFL2, with AFL1 containing fibres in order for the transition from the substrate to become evener. AFL1 contained either NiO or NiO/YSZ powder and YSZ fibres and the former tended to be less cracked and physically deformed. The layers were applied as a homemade paste by a paintbrush. There often needed to be several layers applied in order to achieve a rather smooth surface without holes or fibres sticking up from it. The electrolyte layer was applied by dripping and dip-coating from a homemade solution. The multiple dip-coated samples turned out to have a denser layer but might be more prone to cracking. The cathode was applied in two layers consisting of LSM-YSZ and LSM, which was done with a paintbrush.

SEM was used to visualize the characteristics of the developed SOFC. It showed that the electrolyte layer was semi-dense with some cracks at different areas. Some samples also had a rough texture to it due to an uneven distribution of the AFL.

EDS analysis was performed to investigate the chemical distribution within the substrate, AFL and electrolyte. There was a rather non-uniform distribution of nickel in the substrate.

Performance tests were to be conducted but failed due to malfunctions. It is thus unknown whether or not any of the samples actually work but given the imperfections verified by SEM analysis, it is rather unlikely that the method presented in this thesis is sufficient for a functioning light weighted SOFC.

6 Future work

For future aspirations of continuing this work, this section aims to give further ideas on how to improve the techniques.

Another method for constructing the samples need to be applied in order to achieve better results. A custom made mould for the tubular samples that produces a better substrate surface should be made. This would decrease the thickness of the AFL which in turn would decrease the TECs contribution to the change in physical appearance.

The AFL paste showed some lumps and uneven grinding which in order to achieve a more flat electrolyte layer need to be more homogeneous. This might be achieved by tape casting as to achieve a smoother surface.

Since there was a small amount of nickel in the anode the second impregnation step comprising YSZ or ceria could be replaced by a nickel solution in order to increase the electrical conductivity as well as minimize the difference in TEC. This might however lead to a more coarsening of the nickel grains. Also if coarsening is affecting the overall efficiency an extra nickel impregnation could take place after the electrolyte sintering.

In this project a nickel nitrate solution was used. It was later discovered that the precipitation could have been more homogeneous if urea was added, which would have formed hydroxide ions at 70 °C which in turn would form the solid compound nickel hydroxide, see Formula 4 and 5 below [19].

$$CO(NH_2)_2 + H_2O \rightarrow 2NH_4^+ + 2OH^- + CO \quad (4)$$

$$Ni^{2+} + 2OH^- \rightarrow Ni(OH)_2 \quad (5)$$

Since many of the samples developed a bent geometry, a ceramic press could be applied during the sintering, this might however create cracks.

An investigation of the TEC difference contribution to the physical deformation observed after sintering could be done by heating samples coated with AFL but without any electrolyte to 1400 °C. These samples would thus not be affected by the electrolyte shrinkage.

Since the electrolyte membrane is not completely dense a higher sintering temperature could be used to solve this problem. A higher sintering temperature would however most likely worsen the curvature developed during sintering.

7 References

[1] J. Irvine, P. Connor, Solid Oxide Fuel Cells: Facts and Figures, Solid Oxide Fuel Cells: Past, Present and Future, Green Energy and Technology, 2013, pp. 1-23

[2] N. Minh, T. Takahashi, Science and Technology of Ceramic Fuel Cells, Chapter 1, Introduction, Elsevier, 1995, pp. 1-14

[3] B. Prakash, S. Kumar, S. Aruna, Properties and Development of Ni/YSZ as an Anode Material in Solid Oxide Fuel Cell: A Review, Renewable and Sustainable Energy Reviews, Vol. 36, 2014, pp. 149-179

[4] N. Mahato, A. Banerjee, A. Gupta, S. Omar, K. Balani, Progress in Material Selection for Solid Oxide Fuel Cell Technology: A Review, To appear in: Progress in Materials Science, 2015, pp. 1-437

[5] J. Irvine, P. Connor, Solid Oxide Fuel Cells: Facts and Figures, Alternative Materials for SOFCs, Opportunities and Limitations, Green Energy and Technology, 2013, pp. 163-180

[6] C. Zuo, M. Liu, M. Liu, Sol-Gel Processing for Conventional and Alternative Energy, Chapter 2, Solid Oxide Fuel Cells, Springer, 2012, pp. 7-36

[7] M. Torrell, A. Morata, P. Kayser, M. Kendall, K. Kendall, A. Tarancon, Performance and Long Term Degradation Of 7 W Micro-Tubular Solid Oxide Fuel Cells For Portable Applications, Journal of Power Sources, Vol. 285, 2015, pp. 439-448

[8] M. Andersson, Development of Tubular Solid Oxide Fuel Cells [MSc thesis], Lund University, 2009, pp. 1-34

[9] https://upload.wikimedia.org/wikipedia/commons/thumb/4/42/Solid_oxide_fuel_cell.svg/2000px-Solid_oxide_fuel_cell.svg.png Accessed 2015-10-16

[10] R. Basu, Recent Trends in Fuel Cell Science and Technology, Chapter 1, Introduction to Fuel Cells, Anamaya Publishers, 2007, pp. 1-9

[11] EG&G Technical Services, Inc., Fuel Cell Handbook, Seventh Edition, U.S. Department of Energy, 2004, pp. 7-12

[12] A. Martorana, F. Giannici, A. Longo, Synchrotron Radiation: Basics, Methods and Applications, Springer, 2015, Chapter 27, Synchrotron Radiation and Chemistry - Studies of Materials for Renewable Energy Sources; pp. 697-715

[13] R. Basu, Recent Trends in Fuel Cell Science and Technology, Chapter 11, Solid Oxide Fuel Cells: Principles, Designs and State-of-the-Art in Industries, Anamaya Publishers, 2007, pp. 267-282

[14] M. Gross, J. Vohs, R. Gorte, An Examination of SOFC Anode Functional Layers Based on Ceria in YSZ, Journal of The Electrochemical Society, Vol. 154, 2007, pp. B694-B699

[15] http://www.doitpoms.ac.uk/tlplib/fuel-cells/figures/YSZ-LSM_sml.png and http://www.doitpoms.ac.uk/tlplib/fuel-cells/figures/YSZ-Nickel_sml.png Accessed 2015-10-16

[16] X. Zhang, B. Lin, Y. Ling, Y. Dong, G. Meng, X. Liu, An Anode-Supported Micro-Tubular Solid Oxide Fuel Cell With Redox Stable Composite Cathode, International Journal of Hydrogen Energy, Vol. 35, 2010, pp. 8654-8662

[17] J. Moralesa, J. Vázquez, J. Martíneza, D. Lópeza, P. Núñez, On the Simultaneous Use of La0.75Sr0.25Cr0.5Mn0.5O3–□ As Both Anode and Cathode Material with Improved Microstructure In Solid Oxide Fuel Cells, Electrochimica Acta, Vol. 52, 2006, pp. 278-284

[18] I. Jung, D. Lee, S. Lee, D. Kim, J. Kim, S. Hyun, LSCM–YSZ Nanocomposites For a High Performance SOFC Anode, Ceramics International, Vol. 39, 2013, pp. 9753-9758

[19] S. Jung, C. Lu, H. He, K. Ahn, R.J. Gorte, J.M. Vohs, Influence of Composition and Cu Impregnation Method on The Performance Of Cu/CeO2/YSZ SOFC Anodes, Journal of Power Sources, Vol. 154, 2006, pp. 42-50

[20] R. Gorte, J. Vohs, S. McIntosh, Recent Developments on Anodes for Direct Fuel Utilization in SOFC, Solid State Ionics, Vol. 175, 2004, pp. 1-6

[21] R. Craciuna, S. Park, R. J. Gorte, J. M. Vohs, C. Wang, W. L. Worrell, A Novel Method for Preparing Anode Cermets for Solid Oxide Fuel Cells, Journal of the Electrochemical Society, Vol. 146, 1999, pp. 4019-4022

[22] E. Tsipis, V. Kharton, Electrode Materials and Reaction Mechanisms in Solid Oxide Fuel Cells: A Brief Review, Journal of Solid State Electrochemistry, Vol. 12, 2008, pp. 1039-1060

[23] K. Wincewicz, J. Cooper, Taxonomies of SOFC Material and Manufacturing Alternatives, Journal of Power Sources, Vol. 140, 2005, pp. 280-296

[24] M. Nandasiri S. Thevuthasan, Thin Film Structures in Energy Applications, Chapter 6, State-of-the-Art Thin Film Electrolytes for Solid Oxide Fuel Cells, Springer, 2015, pp. 167-204

[25] Z. Wang, M. Chenga, Y. Donga, M. Zhang, H. Zhang, Anode-Supported SOFC with 1Ce10ScZr Modified Cathode/Electrolyte Interface, Journal of Power Sources, Vol. 156, 2006, pp. 306-310

[26] D. Zhou, G. Zhao, M. Yang, Y. Xia, J. Meng, Effects of MoO3 Amounts on Sintering and Electrical Properties of Ce0.8Nd0.2O1.9, CHEM. RES. CHINESE UNIVERSITIES, Vol. 28, 2012, pp. 9-13

[27] N. Minh, T. Takahashi, Science and Technology of Ceramic Fuel Cells, Chapter 3, Electrical Conduction in Ceramics, 1995, pp. 41-68

[28] R. Basu, Recent Trends in Fuel Cell Science and Technology, Chapter 12, Materials for Solid Oxide Fuel Cells, Anamaya Publishers, 2007, pp. 286-331

[29] M. Backhaus-Ricoult, SOFC - A playground for Solid State Chemistry, Solid State Sciences, Vol. 10, 2008, pp. 670-688

[30] S. Park, J. Ahn, C. Jeong, C. Na, R. Song, J. Lee, Ni-YSZ-Supported Tubular Solid Oxide Fuel Cells with GDC Interlayer Between YSZ Electrolyte and LSCF Cathode, International Journal of Hydrogen Energy, Vol. 39, 2014, pp 12894-12903

[31] A. Hanifi, S. Paulson, A. Torabi, A. Shinbine, M. Tucker, V. Birss, T. Etsell, P. Sarkar, Slip-Cast and Hot-Solution Infiltrated Porous Yttria Stabilized Zirconia (YSZ) Supported Tubular Fuel Cells, Journal of Power Sources, Vol. 266, 2014, 121-131

[32] R. Lewis, SAW'S Dangerous Properties of Industrial Materials, Vol. 3, Tenth edition, John Wiley and sons inc., 2000, pp. 2629-2636

[33] E. Reichelt, M. Heddrich, M. Jahn, A. Michaelis, Fiber Based Structured Materials for Catalytic Applications, Applied Catalysis A: General, Vol. 476, 2014, pp. 78-90

[34] Y. Shiratori, T. Ogura, H. Nakajima, M. Sakamoto, Y. Takahashi, Y. Wakita, T. Kitaoka, K. Sasaki, Study on Paper-Structured Catalyst for Direct Internal Reforming SOFC Fueled by the Mixture of CH4 and CO2, International Journal of Hydrogen Energy, Vol. 38, 2013, pp. 10542-10551

[35] J. Bortolozzi, E. Banús, D. Terzaghi, L. Gutierrez, V. Milt, M. Ulla, Novel Catalytic Ceramic Papers Applied to Oxidative Dehydrogenation of Ethane, Catalysis Today Vol. 216, 2013, pp. 24-29

[36] E. Banús, M. Ulla, M. Galván, M. Zanuttini, V. Milt, E. Miró ,Catalytic Ceramic Paper for the Combustion of Diesel Soot, Catalysis Communications, Vol. 12, 2010, pp. 46-49

[37] http://zircarzirconia.com/products/type-zyf-zirconian-felt/ as well as email contact with their staff. Accessed 2015-10-16

[38] S. Jiang, S. Chan, A Review of Anode Materials Development in Solid Oxide Fuel Cells, Journal of Materials Science, Vol. 39, 2004, pp. 4405-4439

[39] D. Osinkin, N. Bogdanovich, S. Beresnev, V. Zhuravlev, High-Performance Anode-Supported Solid Oxide Fuel Cell With Impregnated Electrodes, Journal of Power Sources, Vol. 288, 2015, pp. 20-25

[40] C. Xia, M. Liu, A Simple and Cost-Effective Approach to Fabrication of Dense Ceramic Membranes on Porous Substrates, Journal of the American Ceramic Society, Vol. 84, 2001, pp. 1903-1905

[41] J. Liu, S. Barnett, Thin Yttrium-Stabilized Zirconia Electrolyte Solid Oxide Fuel Cells by Centrifugal Casting, Journal of American Ceramic Society, Vol. 85, 2002, pp. 3096-3098

[42] J. Cherng, C. Wu, F. Yu, T. Yeh, Anode Morphology and Performance of Micro-Tubular Solid Oxide Fuel Cells Made by Aqueous Electrophoretic Deposition, Journal of Power Sources, Vol. 232, 2013 pp. 353-356

[43] Y. Zhang, J. Liu, J. Yin, W. Yuan, J. Sui, Fabrication and Performance of Cone-Shaped Segmented-In-Series Solid Oxide Fuel Cells, International Journal of Applied Ceramic Technology, Vol. 5, 2008, pp. 568-573

[44] H. Tikkanen, C. Suciu, I. Wærnhus, A. Hoffmann, Examination of the Co-Sintering Process of Thin 8YSZ Films Obtained by Dip-Coating on In-House Produced NiO–YSZ, Journal of the European Ceramic Society, Vol. 31, 2011, pp. 1733-1739

[45] X. Meng, X. Gong, N. Yang, Y. Yin, X. Tan, Z. Ma, Carbon-Resistant Ni-YSZ/CueCeO2-YSZ Dual-Layer Hollow Fiber Anode for Micro Tubular Solid Oxide Fuel Cell, International Journal of Hydrogen Energy, Vol. 39, 2014, pp. 3879-3886

[46] R. Egerton, Physical Principles of Electron Microscopy - An Introduction to TEM, SEM, and AEM, Springer, 2005, pp. 1-189

[47] D. Williams, C. Carter, Transmission Electron Microscopy - A Textbook for Materials Science, Second edition, Springer, 2009, pp. 1-757

[48] http://www.inorganic-chemistry-and-catalysis.eu/files/afbeeldingen/content/Persoonlijke%20paginas/Marjan%20Versluijs/mvsem32.jpg Accessed 2015-10-16

[49] http://www.ualberta.ca/~ccwj/teaching/microscopy/Figs/PNG/electronemission.png Accessed 2015-10-16

[50] C. Singh, V. Krishnan, Synthesis and Characterization of Ni Impregnated Porous YSZ Anodes for SOFCs, Advances in Solid Oxide Fuel Cells IV, Ceramic Engineering and Science Proceedings, Vol. 29, 2008, pp. 173-179

Appendix A

A1 Calculations for the YSZ colloidal solution, from section 3.1.1

To achieve an 8mol% YSZ solution from yttria and zirconia solutions the following calculations were used.

wt% of the colloidal solutions needed:

$n(Y_2O_3) = 8\ mol$

$M(Y_2O_3) = 225{,}8\ g/mol$

$n(ZrO_2) = 92\ mol$

$M(ZrO_2) = 123{,}2\ g/mol$

$m(Y_2O_3) = n(Y_2O_3) * M(Y_2O_3) = 8 * 225{,}8 = 1806\ g$

$m(ZrO_2) = n(ZrO_2) * M(ZrO_2) = 92 * 123{,}2 = 11334\ g$

$$wt\%(Y_2O_3) = \frac{m(Y_2O_3)}{m(Y_2O_3) + m(ZrO_2)} = \frac{1806}{1806 + 11334} = \mathbf{13{,}75}\ \%$$

$$wt\%(ZrO_2) = \frac{m(ZrO_2)}{m(Y_2O_3) + m(ZrO_2)} = \frac{11334}{1806 + 11334} = \mathbf{86{,}25}\ \%$$

The solutions were weighed accordingly and mixed together.

A2 Calculations for the theoretical wt% of NiO during impregnation, from section 3.1.2

A nickel solution was made by mixing 62 g $Ni(NO_3)_2$*$6H_2O$ with 78.2 g H_2O

$m(\mathrm{Ni(NO_3)_2 * 6H_2O}) = 62\ g$

$M(\mathrm{Ni(NO_3)_2 * 6H_2O}) = \ 290.7\ g/mol$

$M(NiO) = 74.7\ \ g/mol$

$$n(\mathrm{Ni(NO_3)_2}) = \frac{m(\mathrm{Ni(NO_3)_2})}{M(\mathrm{Ni(NO_3)_2})} = \frac{62}{290.7} = 0.21\ mol$$

$$n(NiO) = \frac{m(NiO)}{M(NiO)}$$

$$\mathrm{2Ni(NO_3)_2 * 6H_2O} \rightarrow 2NiO + 4\ NO_2 + O_2$$

The chemical equation above implies that $n(\mathrm{Ni(NO_3)_2}) = n(NiO)$

This gives the following expression:

$$\frac{m(\mathrm{Ni(NO_3)_2})}{M(\mathrm{Ni(NO_3)_2})} = \frac{m(NiO)}{M(NiO)} \rightarrow m(NiO) = \frac{m(\mathrm{Ni(NO_3)_2}) * M(NiO)}{M(\mathrm{Ni(NO_3)_2})} = \frac{62 * 74.7}{290.7} = 15.9\ g$$

The amount of water in the solution: $m(H_2O) = 78.2\ g$

$$m(solution) = m(H_2O) + m(NiO) = 78.2 + 15.9 = 94.1\ g$$

$$wt\%(NiO) = \frac{m(NiO)}{m(solution)} = \frac{15.9}{94.1} \sim \mathbf{17}\ \%$$

A3.1 Calculation of $Ni(NO_3)_2*6H_2O$ concentration used in the experiments, from section 4.1.2

$\rho(\mathrm{Ni(NO_3)_2 * 6H_2O}) = 2.05\ \mathrm{g/cm^3}$

$$V(\mathrm{Ni(NO_3)_2 * 6H_2O}) = \frac{m(\mathrm{Ni(NO_3)_2 * 6H_2O})}{\rho(\mathrm{Ni(NO_3)_2 * 6H_2O})} = \frac{62}{2.05} = 30.2\ cm^3$$

$V(H_2O) = 78\ cm^3$

$V_{tot} = V(H_2O) + V(\mathrm{Ni(NO_3)_2 * 6H_2O}) = 30.2 + 78 = 108.2\ cm^3$

$$c(\mathrm{Ni(NO_3)_2 * 6H_2O}) = \frac{n(\mathrm{Ni(NO_3)_2 * 6H_2O})}{V_{tot}} = \frac{0.21}{0.1082} = 1.97 \approx \boldsymbol{2\ mol/L}$$

A3.2 Calculations of the average vol% of nickel in the substrates, from section 4.1.2

$2NiO \rightarrow 2Ni + O_2$

$m(NiO) = 100\ g$

$M(NiO) = 74.7\ g/mol$

$M(Ni) = 58.7\ g/mol$

According to the formula above, the following expression can be written:

$$n(Ni) = n(NiO) = \frac{m(NiO)}{M(NiO)} = \frac{100}{74.7} = 1.34\ mol$$

$m(Ni) = n(Ni) * M(Ni) = 1.34 * 58.7 = 78\ g$

This means that 78% of the NiO mass becomes Ni. Since the average NiO amount is 10% the amount Ni thus become 8wt%.

The following calculations are based on 100g sample.

$\rho(Ni) = 8.9\ g/cm^3$

$\rho(NiO) = 6.67\ g/cm^3$

$\rho(substrate) = \rho(YSZ) = 6.1\ g/cm^3$

$$V(Ni) = \frac{m(Ni)}{\rho(Ni)} = \frac{8}{8.9} = 0.90\ cm^3$$

$m(substrate) = 1 - m(NiO) = 90\ g$

$$V(substrate) = \frac{m(substrate)}{\rho(substrate)} = \frac{90}{6.1} = 14.7\ cm^3$$

$$Vol\%(Ni) = \frac{V(Ni)}{V(substrate)} = \frac{0{,}9}{14{,}7} = \mathbf{6\ vol\%}$$

Appendix B

Chemical and materials information

10-YSZ and alumina ceramic fibre paper were bought by Zircar Zirconia, Inc.

Ethyl cellulose was received as a sample by Dow chemicals as the substance Ethocel Standard 45.

Terpineol (anhydrous mixture of isomers), Poly Vinyl Butyrate (Butvar® B-98) and Triton X-100 were bought from Sigma Aldrich.

NiO powder, YSZ powder and Ni-GDC powder were bought from the company NexTech Materials, their specifications are given in the table below.

Table 9. Surface area and particle size of purchased powders according to the supplier, NexTech Materials.

Substance	**Surface area / m^2*g^{-1}**		**Particle size, d_{50} / µm**	
	Expected	Measured	Expected	Measured
NiO powder	3-7	3.1	0.5-1.5	0.66
YSZ powder	6-9	7.6	0.5-0.7	0.51
Ni-GDC powder	4-8	4.8	-	-

The colloidal solutions were bought from Nyacol®. Their properties can be seen in the table below.

Table 10. Technical information for the colloidal solutions, as given by the company Nyacol®.

Colloidal solution	**wt%**	**Colloid size / nm**	**pH**	**Viscosity / cPa**
Nyacol® Y2O3	14	10	7.0	10
Nyacol® ZRO2ACT	20	5-10	3.5	10
Nyacol® CEO2(AC)	20	10-20	3.0	10

Ethanol, deionized water, as well as other chemicals were taken from the chemical supply at Catator.

Appendix C

Experimental details from section 3.2.3 and 3.2.4

AFL1

Two different pastes were made. One consisting of NiO powder and one with NiO-YSZ powder, see Table 6 and 7 respectively. The NiO-YSZ powder mixture was made in the following way: 123g NiO powder and 82g YSZ powder was ball milled at 399 rpm for 20 h with a powder/ball weight ratio of 50/50.

The following method was applied to both the NiO and the NiO-YSZ fibre pastes. The fibre paste was made by first grinding the YSZ fibre for 5 min. The NiO-YSZ / NiO was added followed by 15 min of grinding. This dry mix was then added to a beaker containing the ink vehicle and stirred manually for 5 min. An ultra-sonic bath was incorporated for 1h with a 5 min stirring break outside the bath after 30 min. The paste was matured for 24 h followed by 5 min stirring and ultra-sonication for 1 h.

Table 11. Ingredient list for the two different fibre pastes used for the AFL1.

	NiO powder / g	NiO-YSZ powder / g	YSZ fibre / g	Ink vehicle / g
NiO fibre	3.236	-	3.227	3.234
NiO-YSZ fibre	-	3.072	3.007	3.045

AFL2

The paste was ball-milled in order to make a more homogeneous solution. The recipe is shown in the table below. After 66 h of ball-milling the paste was too thick and 10 ml ethanol was added followed by 48 h of ball-milling after which the paste looked good.

Table 12. AFL2 paste recipe.

Powder	**Solvents**		**Binders**		**Stabilizer**
NiO-YSZ / g	Terpineol / g	Ethanol / ml	Poly vinyl butyrate / g	Ethyl cellulose / g	Triton X-100 / g
66	33	10	1.5	1.5	0.5

Electrolyte

The electrolyte solution was ball-milled for about 24 h at 399 rpm using a ball to media weight ratio of 2. The recipe is given in the table below.

Table 13. Electrolyte solution recipe.

Powder	Solvent		Binder	Stabilizer
YSZ powder / g	Ethanol / g	Terpineol / g	Ethyl cellulose /g	Triton X-100 / g
10	85.5	4.3	0.27	0.5

Appendix D

Detailed elemental spectrum maps from section 4.2.2

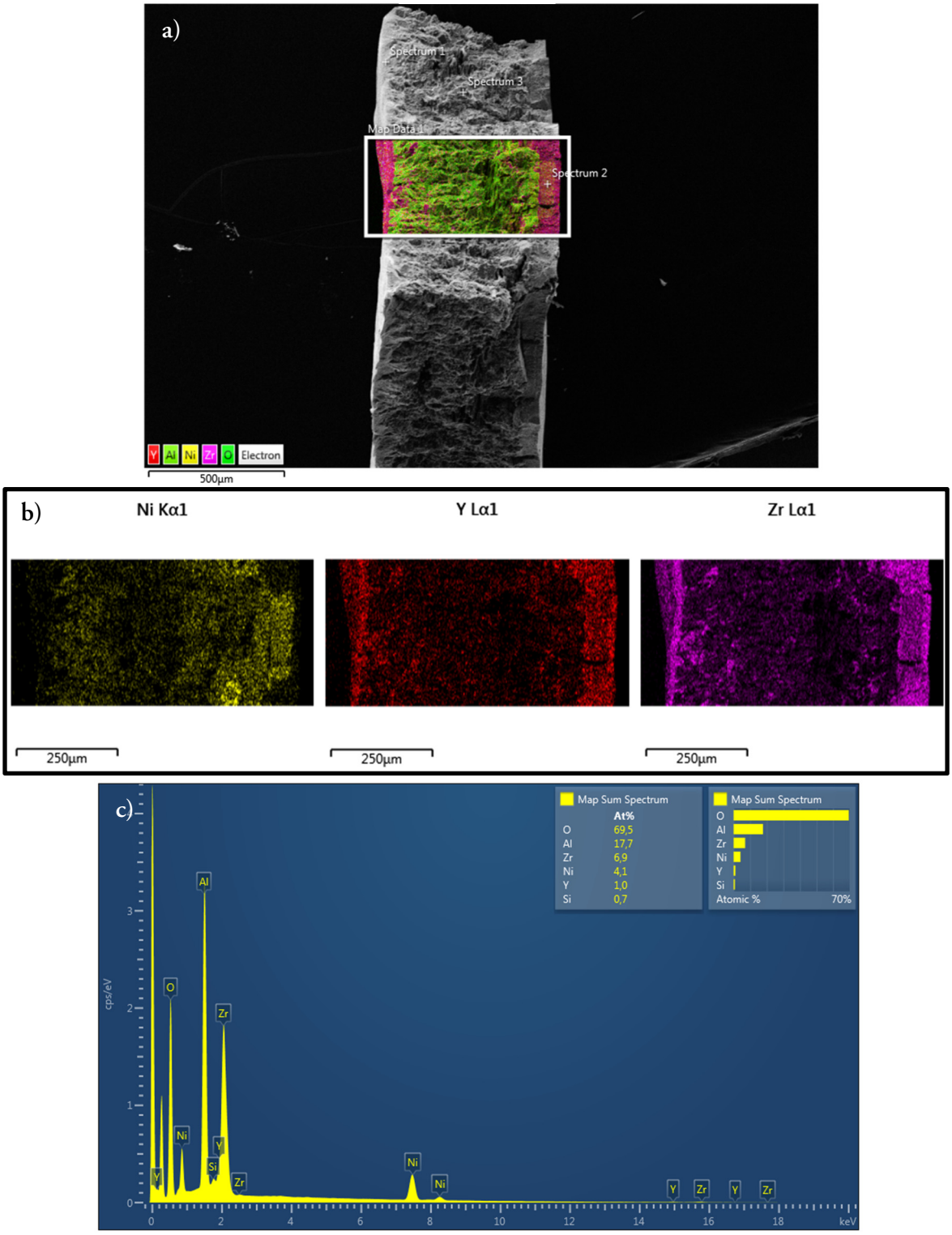

Figure 26. In a) an EDS mapping of an area that comprises the whole thickness of the sample including a cross-section of the electrolyte. The distribution of nickel, yttrium and zirconium within the area can be seen in b) and their relative spectra are depicted in c).

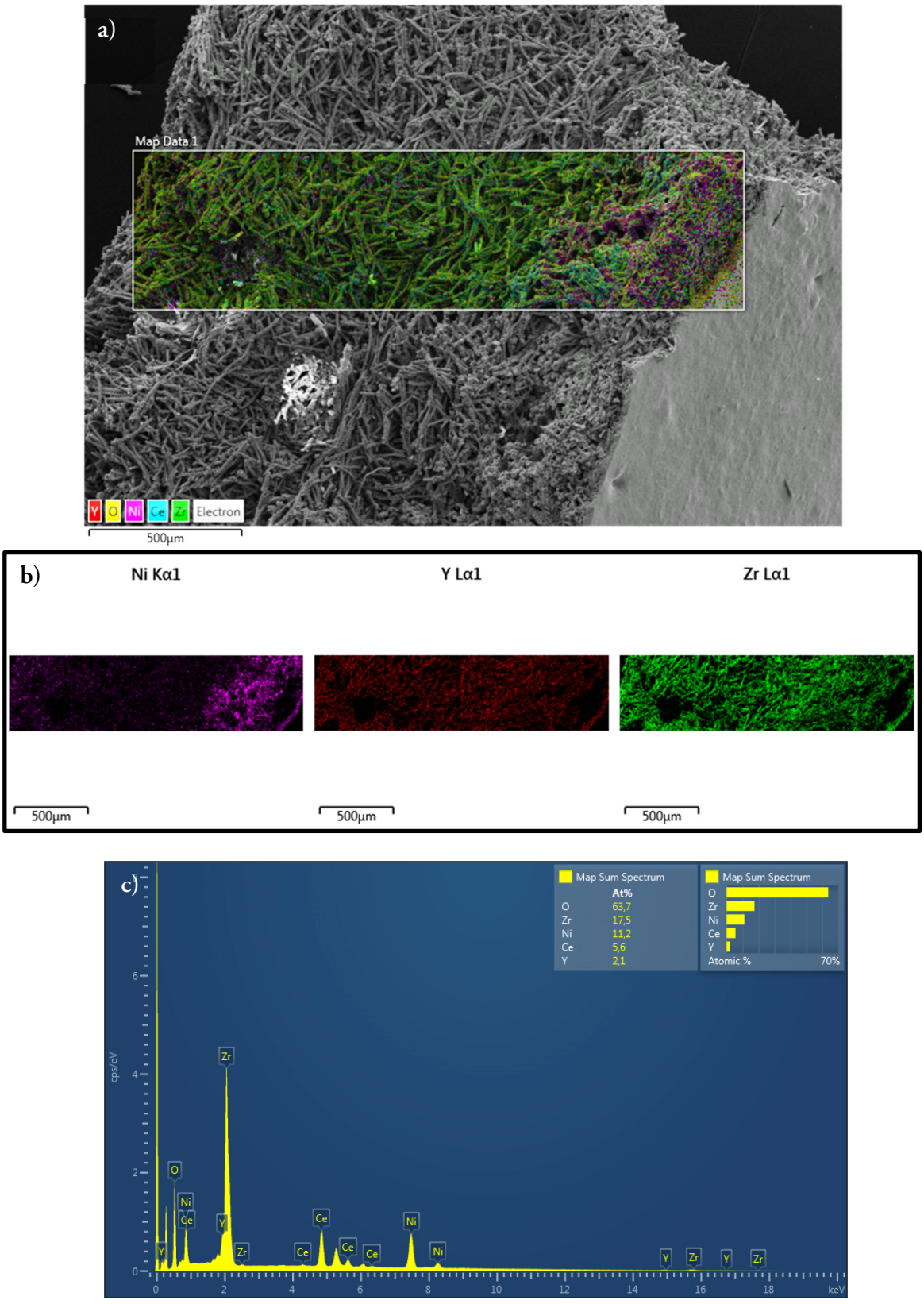

Figure 27. In a) an EDS mapping of an area that comprises the whole thickness of the sample can be seen. The distribution of nickel, yttrium and zirconium within the area can be seen in b) and their relative spectra are depicted in c).

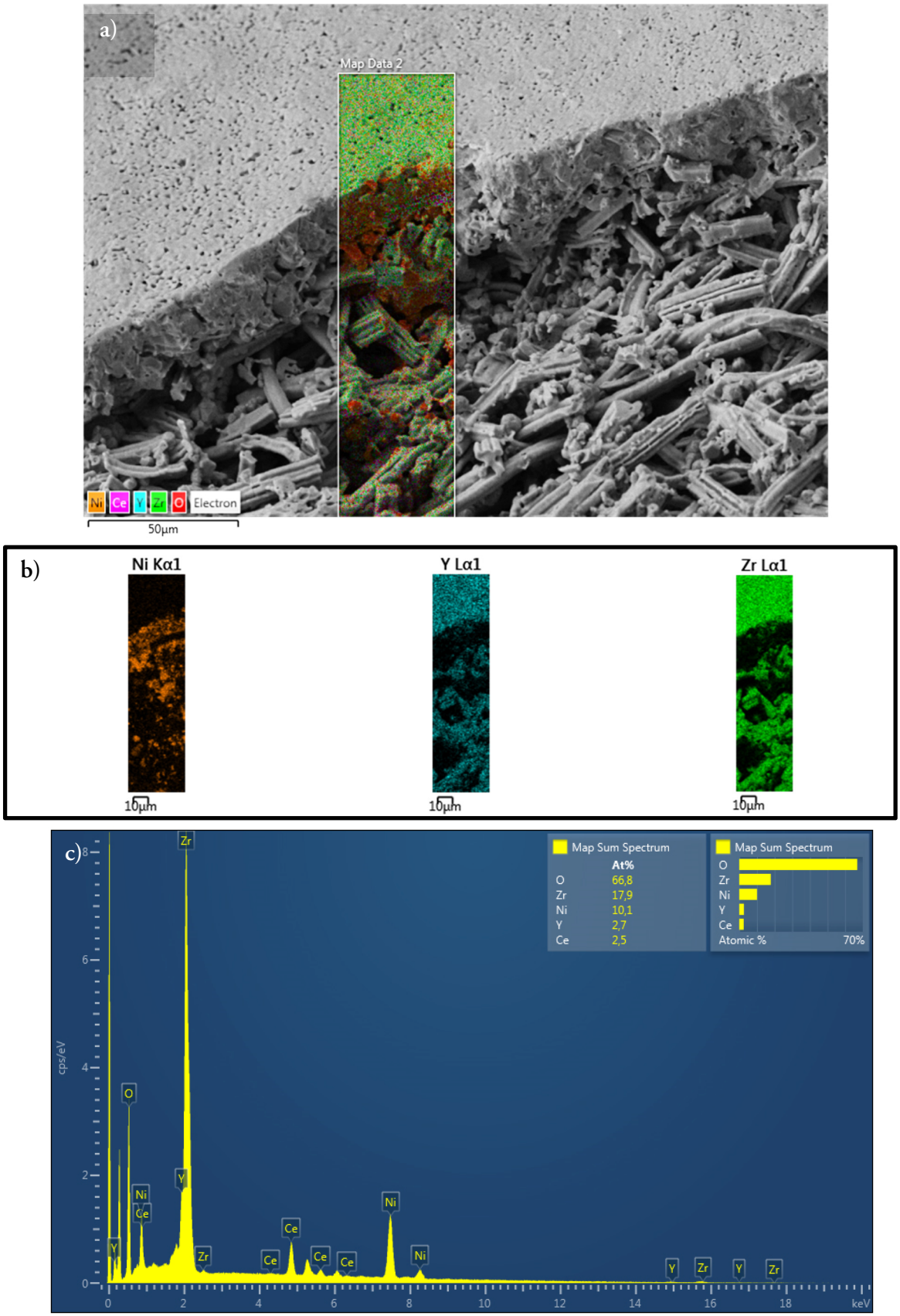

Figure 28. In a) an EDS mapping of an area that comprises the whole thickness of the sample including the electrolyte surface can be seen. The distribution of nickel, yttrium and zirconium within the area can be seen in b) and their relative spectra are depicted in c).